Kaolinite Dissolution and Precipitation Kinetics at 22°C and pH 4

Li Yang
Carl I. Steefel

Earth Sciences Division
Lawrence Berkeley National Laboratory

In Press, Geochimica et Cosmochimica Acta

August 5, 2008

ABSTRACT

Dissolution and precipitation rates of low defect Georgia kaolinite (KGa-1b) as a function of Gibbs free energy of reaction (or reaction affinity) were measured at 22°C and pH 4 in continuously stirred flowthrough reactors. Steady state dissolution experiments showed slightly incongruent dissolution, with a Si/Al ratio of about 1.12 that is attributed to the re-adsorption of Al on to the kaolinite surface. No inhibition of the kaolinite dissolution rate was apparent when dissolved aluminum was varied from 0 and 60 μM. The relationship between dissolution rates and the reaction affinity can be described well by a Transition State Theory (TST) rate formulation with a Temkin coefficient of 2

$$R_{diss}\left(\mathrm{mol}/\mathrm{m^2 s}\right) = 1.15\times10^{-13}\left[1-\exp\left(\frac{-\Delta G}{2RT}\right)\right].$$

Stopping of flow in a close to equilibrium dissolution experiment yielded a solubility constant for kaolinite at 22°C of $10^{7.57}$.

Experiments on the precipitation kinetics of kaolinite showed a more complex behavior. One conducted using kaolinite seed that had previously undergone extensive dissolution under far from equilibrium conditions for 5 months showed a quasi-steady state precipitation rate for 105 hours that was compatible with the TST expression above. After this initial period, however, precipitation rates decreased by an order of magnitude, and like other precipitation experiments conducted at higher supersaturation and without kaolinite seed subjected to extensive prior dissolution, could not be described with the TST law. The initial quasi-steady state rate is interpreted as growth on activated sites created by the dissolution process, but this reversible growth mechanism could not be maintained once these sites were filled. Long-term precipitation rates showed a linear dependence on solution saturation state that is generally consistent with a two dimensional nucleation growth mechanism following the equation

$$R_{ppt}\left(\mathrm{mol}/\mathrm{m^2 s}\right) = 3.38\times10^{-14}\exp\left[-\frac{181776}{T^2\ln\Omega}\right].$$

Further analysis using Synchrotron Scanning Transmission X-ray Microscopy (STXM) in Total Electron Yield (TEY) mode of the material from the precipitation experiments showed spectra for newly precipitated material compatible with kaolinite. An idealized set of reactive transport simulations of the chemical weathering of albite to kaolinite using rate laws from HELLMANN and TISSERAND (2006) and this study respectively indicate that while pore waters are likely to be close to equilibrium with respect to kaolinite at pH 4, significant kaolinite supersaturation may occur at higher pH if its precipitation rate is pH dependent.

INTRODUCTION

The kinetics of mineral dissolution and precipitation are critical to the interpretation and modeling of geochemical processes at Earth's surface. Some of the most important phases in this regard are the clay minerals, of which kaolinite is perhaps the most important. Kaolinite plays an important role in regulating soil and subsurface aquifer solution chemistry, and its precipitation may even control the extent of undersaturation with respect to primary dissolving phases like feldspar (STEEFEL and VAN CAPPELLEN, 1990; ALEKSEYEV et al., 1997; ZHU et al., 2004; MAHER et al., 2006). A number of studies of kaolinite dissolution have been carried out previously (CARROLL-WEBB and WALTHER, 1988; CARROLL and WALTHER, 1990; NAGY et al., 1990; NAGY et al., 1991; XIE and WALTHER, 1992; WIELAND and STUMM, 1992; GANOR et al., 1995; DEVIDAL et al., 1997; HUERTAS et al., 1999; METZ and GANOR, 2001; CAMA et al., 2002; CAMA and GANOR, 2006). However, most of those studies focused on the determination of the pH and temperature dependence of the dissolution rates in far from equilibrium, highly undersaturated dilute solutions. The variation of dissolution rates with pH was considered to be related to the adsorption of protons or hydroxyls to the specific sites on mineral surfaces, with the suggestion that edge sites on the kaolinite dominated the rate (CARROLL-WEBB and WALTHER, 1988; WIELAND and STUMM, 1992). Although those studies provided general information on the mechanisms of kaolinite dissolution, the data are of limited use for predicting the kinetic reactions in natural systems, since pore fluids in soils or aquifers do not remain indefinitely far from equilibrium.

Compared to dissolution studies, there are relatively few studies on the kinetics of kaolinite precipitation and most of these studies were performed at temperatures well above those of the

Earth's surface. Nagy and co-workers (NAGY et al., 1991; NAGY and LASAGA, 1993) studied the kinetics of kaolinite dissolution and precipitation at pH 3 and 80°C. Their studies showed a linear dependence of dissolution/precipitation rates on reaction affinity (or Gibbs free energy) at near equilibrium conditions and obtained a Temkin coefficient of 1 for the dissolution reactions using a Transition State Theory rate formulation. Other studies focused on the kinetics of kaolinite precipitation/dissolution at hydrothermal conditions and also indicated that principle of detailed balancing was applicable under close to equilibrium conditions (SOONG and BARNES, 1992; HUANG, 1993). DEVIDAL et al (1997) studied the dissolution and precipitation kinetics of kaolinite as a function of chemical affinity at hydrothermal conditions (150°C, 40 bars) and concluded that the variation of kaolinite dissolution/ precipitation rates with reaction chemical affinity can be described by a coupled Transition State Theory and Langmuir adsorption model, with the rate controlled by the decomposition of a silica-rich/aluminum deficient precursor. However, it remains unclear whether these experiments carried out under hydrothermal conditions are directly applicable to the lower temperatures and pressures of near-surface geologic environments. Therefore, it is important to directly measure the kaolinite dissolution/precipitation rates at ambient temperature and pressure conditions where possible. As is the case with dissolution, it is also essential to determine the dependence of the rate on reaction affinity.

To describe the rates of dissolution and precipitation as a function of reaction affinity, Transition State Theory (TST) has been widely used as a theoretical framework. Recently, Lasaga and Luttge (LASAGA and LUTTGE, 2001; LASAGA and LUTTGE, 2003) proposed an alternative model for mineral dissolution under close to equilibrium conditions that involves step wave dissolution. Dove et al (DOVE et al., 2005) also recently applied the mechanisms of classical crystal growth theory to explain quartz and aluminosilicate dissolution behavior with a model that did not follow the classical TST relationship.

This paper reports the first attempt to measure the kinetics of kaolinite dissolution and precipitation at ambient temperature and pressure (22°C and 1 bar) and at a pH of 4. Well crystallized low defect Georgia kaolinite (KGa-1b from the Clay Minerals Society) was used as seed material to determine dissolution/precipitation rates as a function of reaction affinity and variable Al and dissolved Si concentration. Dissolution and precipitation rates were evaluated as

to their reversibility and congruency, and the applicability of various rate laws was investigated. Using the kaolinite precipitation rate that was determined in this study together with a rate law for albite (plagioclase feldspar) dissolution proposed by HELLMANN and TISSERAND (2006) that was adjusted to 25ºC, a simple set of reactive transport calculations of chemical weathering are used to evaluate the extent to which kaolinite precipitation rates are fast enough to maintain the pore water solution close to equilibrium with respect to kaolinite.

THERMODYNAMIC AND KINETIC BACKGROUND

The overall kaolinite dissolution and precipitation kinetics under acidic conditions can be expressed as

$$Al_2Si_2O_5(OH)_4 + 6H^+ \text{ €} \quad 2Al^{3+} + 2H_4SiO_4 + H_2O\,. \tag{1}$$

The equilibrium constant for the reaction is given by

$$K_{eq} = \frac{a^2_{Al^{3+}} a^2_{H_4SiO_4}}{a^6_{H^+}}, \tag{2}$$

where a_i represents the thermodynamic activity of the dissolved species and the activities of water and kaolinite are assumed to = 1.

The dissolution and precipitation rates, $R_{diss/ppt}$ (mol. m^{-2} s^{-1}), in a well-mixed flowthrough reactor are determined at steady state from the change in Al and Si according to the following expression

$$R_{diss\,/\,ppt}\left(\text{mol}/\text{m}^2\text{s}\right) = \frac{Q}{\eta_i A}\left[C_{i,in} - C_{i,out}\right], \tag{3}$$

where Q is the volumetric flow rate of the input fluid (L/s), $C_{i,\,out}$ and $C_{i,\,inp}$ are the concentrations of component i (Al or Si in the case of kaolinite) in the output and input solutions, respectively (mol/L), η_i is the stoichiometric coefficient of component i in the reaction (2 in the case of both Al and Si), and A is the surface area (m^2). Steady state has been defined as where the output Al or Si concentration was stable with less than 10% variation for at least one reactor volume. This interval is typically characterized by multiple data points. The dissolution (or precipitation) rates were calculated based on the average results from the data in the steady state interval.

The degree of solution saturation state with respect to the kaolinite dissolution/ precipitation reaction is expressed in terms of the Gibbs free energy of reaction, ΔG_r

$$\Delta G_r = RT \ln\left[\frac{IAP}{K_{eq}}\right] = RT \ln\left[\Omega\right] \quad (4)$$

where R is the gas constant, T is the absolute temperature (K), IAP and K_{eq} are the ion activity product and the equilibrium constant respectively, and $\Omega = IAP/K_{eq}$. To describe the activities of the solutes involved in the reaction accurately, it was necessary to carry out a calculation of the distribution of aqueous species. For this purpose, the geochemical computer code PHREEQC was used (PARKHURST and APPELO, 1999). Al and Si species and their hydrolysis constants used in the calculation are listed in Table 1.

MATERIALS AND METHODS

Source clay and pre-treatment

Kaolinite used in this study is a low defect Georgia kaolinite, KGa-1b, purchased from the Clay Minerals Society. Samples were cleaned prior to dissolution and precipitation experiments to remove amorphous oxy-hydroxide material by washing with 1M NaCl/HCl at pH 3 until the supernatant pH reached 3, followed by repeatedly rinsing with ultra-pure H_2O (18.3 MΩ.cm) and vacuum filtration through 0.1 μm polycarbonate membrane filter until pH > 5. The cleaned and rinsed samples were then dried at 50°C in the oven, gently crushed and stored in a HDPE bottle. The BET surface area determined for the pre-treated kaolinite samples was 11.83± 0.02 m^2 /g (Micrometrics TriStar 3000 measured with N_2), which is similar to the value of 10.05± 0.02 m^2 /g reported by the Clay Mineral Society.

Experimental approach

Experiments were carried out using a well-stirred flowthrough reactor (70 mL in volume) manufactured by Advantec/MFS, Inc. held at room temperature (22±2°C) and pressure. Between 1 and 2 g of kaolinite was allowed to react with a continuously injected fluid of fixed input composition. The flow rates were controlled by a HPLC or syringe pump and ranged from 0.05ml/min to 0.001 mL/min, yielding a residence time within the stirred cell ranging from a minimum of 24 hours to a maximum of 48 days. Stirring of kaolinite and the fluid was controlled by a magnetic stir plate placed directly beneath the reactor using a Teflon-coated stir bar that was mounted on a hanging rod to avoid grinding of the kaolinite

within the reactor. Solutions were filtered through the base of the stirred cell reactor with a 0.45 μm nylon and 0.1 μm polycarbonate membrane filter in sequence. Filtered effluents were collected in clean low density polyethylene bottles and polypropylene vials. The solutions collected were analyzed for total Al and Si by inductively coupled plasma optical emission spectroscopy (ICP-OES, Perkin Elmer DV5300). Each sample was analyzed with 5 replicates. The 95% confident level was reported according to student *t* test value for standard deviations based on the 5 replicates.

Flow rates as low as 1 μL/minute were used to produce a measurable change in concentration in the reactor effluent. A micro-PFA self-aspirating nebulizer with 50 μL/minute sample injection tubing was used with the ICP-OES to analyze the small sample volumes that resulted from the low flow rates (typically about 200 μL for the 5 replicates) so as to provide accurate analytical results. The solution pH was measured with an Acute® pH electrode with a reported accuracy of 0.02 pH unit for samples in experiments with high fluid flow rates. For a small number of samples collected at very slow flow rates in precipitation experiments where the effluent volume was less, the pH was measured with an Orion® Micro-pH electrode. After pH measurement, all samples were acidified with 2% ultra-pure HNO_3 (J. T. Baker®) before ICP-OES analysis. Before beginning a new experiment with the same kaolinite, the stirred cell was flushed with new input stock solution for about 2-3 pore volumes at a high flow rate (~0.5 ml/min) to eliminate residues of the previous stock solution.

Input stock solutions for aluminum were made by diluting aluminum ICP standard solution (from CPI®, source material $AlCl_3$ dissolved in ultrapure HNO_3) with 18.3 MΩ.cm deionized water. Silica stock solution was made of reagent grade $Na_2SiO_3.9H_2O$ (from J.T. Baker®) dissolved in deionized water. The input stock solution was adjusted to the specified pH with diluted ultrapure HNO_3 or reagent grade NaOH solution. The ionic strength of the input solution was adjusted to 0.01M using reagent grade $NaNO_3$ (Alfa Aesar®). Stock solutions were checked periodically for their purity and fresh stock solutions were made every month.

A total of six different target stock solution compositions were used as input to the flowthrough reactors in this study, three for dissolution and three for precipitation (Table 2). The target compositions of input solutions, coupled with varying fluid flow speeds, were designed to cover a wide range of reaction affinity with respect to kaolinite. To represent the variations in effluent solution chemistry, the experimental duration time of each individual experiment was converted to pore volumes according to the volume of the stir cell reactor used in this study (70 ml) and corresponding fluid flow rates. The effluent solution chemistry was plotted as ΔC_{Al} and ΔC_{Si} (ΔC_{Al} and ΔC_{Si} are defined as C_{out}-C_{in} for samples in

dissolution experiments and as C_{in}-C_{out} for samples in precipitation experiments) against pore volumes for all experimental results to facilitate comparisons of experimental results using different input stock solutions.

To determine the kaolinite solubility constant at 22°C, flow was stopped in a dissolution experiment run close to equilibrium and the solution was allowed to equilibrate for an additional period of one week. The solubility constant is also bracketed more broadly by the results of the dissolution and precipitation experiments.

The error propagation in the calculated ΔC_{Al} and ΔC_{Si} in the effluent as well as the error in the rates were estimated using the following equations (MILLER and MILLER, 1993)

$$\sigma_{\Delta C} = \sqrt{\sigma^2_{C_{i,out}} + \sigma^2_{C_{i,in}}} \tag{5}$$

$$\frac{\sigma_r}{r} = \sqrt{\left(\frac{\sigma_{\Delta C}}{\Delta C}\right)^2 + \left(\frac{\sigma_A}{A}\right)^2 + \left(\frac{\sigma_Q}{Q}\right)^2} \tag{6}$$

where $\sigma_{r,}$ is the uncertainty in the calculated rate, $\sigma_{\Delta c}$ represents the uncertainties of the calculated Al or Si concentration difference (ΔC) between input and output solution, $\sigma_{Ci,\ out}$ and $\sigma_{Ci,\ inp}$ are the Al or Si concentration uncertainties (reported at 95% confidence level) in the output and input solutions, respectively, and σ_A and σ_Q are the uncertainties in the surface area and pumping speed, respectively.

Since the differences between the input and output solution concentrations of Al and Si were used for kinetic rate calculations, it was essential to analyze solute concentrations with a high degree of accuracy. Therefore, great efforts were made to obtain high accuracy sample analysis. Even so, it is still difficult to achieve less than 1% relative standard deviation (RSD) during sample analysis, especially for samples with high Si and Al concentrations. Since all data are reported at the 95% confident level, this corresponds to about 1.24 RSD as uncertainties (based on a student *t* test value for 5 replicate samples). For samples with high Si or Al in the input stock solution, the error propagation will further amplify the uncertainties in the calculated ΔC_{Al} and ΔC_{Si} values. Therefore, experimental results having the smallest uncertainties in the calculated ΔC_{Al} and ΔC_{Si} were those with zero Al and Si in the input stock solution. In order to bring the saturation states of the input solutions close to equilibrium with respect to kaolinite while keeping them undersaturated with respect to gibbsite, however, the composition of input stock solutions needed to have a high Si/Al ratio in most experiments. This resulted in large uncertainties in the ΔC_{Si} values compared to the corresponding ΔC_{Al} in the precipitation and close to equilibrium dissolution

experiments. Therefore, effluent Al concentrations coupled with solution pH were used as the main criteria to determine if the steady state had been reached. For the same reason, the steady state change in Al concentration between the input and output solution was used for determination of reaction rates in all experiments to minimize the uncertainties in the rates that are calculated. Although the net change in Al concentration showed a larger uncertainty than did the Si data in the KGa-D3 dissolution experiment because of high Al in the input stock solution, the dissolution rate was still calculated based on Al data to keep this experiment comparable to the other experiments.

Characterization of precipitation samples

Samples in the precipitation experiments were characterized by synchrotron X-ray powder diffraction (SXRD) and Scanning X-ray Transmission Microscopy (STXM) methods at the Advanced Light Source (ALS) of Lawrence Berkeley National Laboratory. In the synchrotron X-ray diffraction study, a few drops of precipitation sample wet paste were transferred to 0.6 mm inner diameter glass capillary tubes or mounted on a cellulose tape and examined on Beamlines 11.3.1 and 10.3.2 at the ALS with a monochromatic X-ray of 0.7293 Angstrom wavelength. In addition to the SXRD study, a small amount of solid material (original kaolinite plus new precipitate) from the precipitation experiments was mounted on silicon nitride windows (manufactured by Silson, Ltd) and further examined by synchrotron STXM on Beamline 11.0.2 at the Advanced Light Source. The Al spectrum of standard Georgia kaolinite (from the Clay Minerals Society) and gibbsite (from Ward Scientific) were also collected for comparison with those from the precipitation experiments. In order to examine only the surface layer of the reacted samples, the spectrum was collected in Total Electron Yield (TEY) mode. In TEY mode, instead of recording the transmitted or fluorescence X-rays, the elastic electrons generated by incident X-ray are recorded as a function of the energy of incident X-ray. This technique is surface sensitive and has a probing depth of only about 3 nm at the Al K edge (ABBATE et al., 1992; EBEL et al., 1994).

RESULTS

Equilibrium solubility

In order to calculate accurately the Gibbs free energy for kaolinite, we found it necessary to measure the solubility of the actual kaolinite used in this study at 22°C. For this purpose, the inlet line of a sample from a close to equilibrium dissolution experiment was disconnected at the end of the experiment and allowed to further equilibrate with the kaolinite sample for about 1 week as stirring continued. The two sampling points that were measured in this way had very

similar aqueous Al and Si compositions and showed only slight differences in the solution pH within the uncertainties of the pH measurement. Accordingly, the averaged results were used to calculate the kaolinite solubility constant. The equilibrium solubility determined in this way was $10^{7.57}$ at the experimental temperature of 22 °C (Table 3). May and co-workers studied the solubility of Dry beach Georgia kaolinite and determined its solubility to be $10^{7.45}$ at 25°C (MAY et al., 1986). Nagy and co-workers derived the equilibrium solubility of Twiggs County Georgia Kaolinite as $10^{3.75}$ at 80 °C (NAGY et al., 1991). Using the Van't Hoff equation with an enthalpy change of -35.3 kcal/mol (taken from PHREEQC database, PARKHURST and APPELO, 1999) for the kaolinite dissolution reaction, the equilibrium solubility value determined in this study is in close agreement with the extrapolated results of MAY et al (1986) ($10^{7.7}$ at 22°C) and the extrapolated data from NAGY et al (1991) ($10^{8.04}$ at 22°C). The Gibbs free energies for all of the kinetic experiments reported here were calculated based on the equilibrium solubility derived in this study.

Dissolution experiments

Dissolution experiments were conducted with three separate kaolinite samples (referred to as KGa-D1, KGa-D2, KGa-D3 in Table 4) under five different conditions. Figures 1 through 3 show the variations in ΔC_{Al} and ΔC_{Si} in the effluent of all dissolution experiments over time. Typically, steady state was reached within 10 pore volumes (about 200 hours) in newly started dissolution experiments. In contrast, it required much less time (about 5 pore volumes) to reach a second steady state when only flow rates were adjusted in experiments started from a previously established steady state.

It should be noted that during initial experimental setup, the KGa-D1 sample was used to test the flow through reactor configurations and to verify sample analysis protocols. Thus, it had been pre-reacted in the flowthrough reactor with stock solution 1 and 2 for about 5 months before the start of experiments documented here. This extended dissolution may have affected the character of the kaolinite surface relative to other experiments that had no such extended dissolution period far from equilibrium. The KGa-D1 dissolution experiments were conducted with 2g of kaolinite, which was first dissolved at far from equilibrium conditions with stock solution 1 (no Si, no Al) for about 20 pore volumes until steady state had been established (referred to as dissolution

experiment KGa-D1a). Then the input solution was switched to stock solution 2 (0.5mM Si, no Al), which was designed to measure kaolinite dissolution rates closer to equilibrium (KGa-D1b). One gram of kaolinite was used at the start of all other dissolution experiments. In experiment KGa-D2, the kaolinite sample was first dissolved with stock solution 2 at close to equilibrium condition for about 12 pore volumes until a steady state had been reached (KGa-D2a). Then, the fluid flow rate was decreased by a factor of 5 to bring the system closer to equilibrium (KGa-D2b). The KGa-D3 dissolution experiment was conducted with input stock solution 3 (60μM Al, no Si) to measure the dissolution rates at conditions moderately far from equilibrium (ΔG = -16.4 kJ/mol). The effluent solution in this experiment reached steady state after approximately 8 pore volumes.

As shown in Figures 1-3 and Figure 4, all dissolution experiments showed slightly incongruent Si/Al release at steady state, with a preferential release of Si. Although the dissolution experiments with high Si in the input solutions had larger uncertainties in the effluent ΔSi concentration, it can be seen that generally effluent ΔSi was larger than the corresponding ΔAl within the experimental uncertainty. Dissolution experiment KGa-D1a was conducted with an input solution having no Al and Si, and thus should have had a minimum uncertainty in the ΔSi and ΔAl measured. It still showed slightly incongruent dissolution with a Si/Al ratio of about 1.12 in the steady state effluent (Figure 5). However, the increase of pH in the effluent of all dissolution experiments was generally congruent, with the corresponding Al release at steady states within experimental uncertainties (Figure 4).

Precipitation experiments

Precipitation experiments were conducted with kaolinite that had previously been used in dissolution experiments. Since the precipitation of kaolinite is very slow at 22°C, a syringe pump was used to generate a very low flow rate in the precipitation experiments so as to produce measurable differences between the input and output solutions. As a result, it generally took more than one month for the precipitation experiments to reach steady state, with the exception of experiment KGa-P1a. Figure 6-8 show the variation of effluent ΔC_{Al} and ΔC_{Si} for all precipitation experiments as a function of time. Experiments KGa-P2 and KGa-P3 show a deficiency of about 0.03 pH units (Figure 4) relative to stoichiometric precipitation that is likely

the result of the use of a micro-pH electrode in these experiments. Otherwise, the precipitation experiments show stoichiometric decrease of Si, Al, and pH.

KGa-1P precipitation experiment, which was begun with kaolinite used in a dissolution experiment that lasted over 5 months, was noteworthy in showing two quasi-steady states during the course of experiment (Figure 6). The first quasi-steady state was reached after 4 pore volumes (about 95 hours) and lasted an additional 4.5 pore volumes (or about 105 hours). During this period, the effluent solution Si and Al showed continuous stoichiometric precipitation accompanied by a congruent pH drop (Figure 6A). However, after a total of 8.5 pore volumes (or 200 hours), these relatively rapid precipitation rates disappeared and the difference between input and output solution Si and Al concentrations was not measurable. At this point, the fluid flow speed was decreased by a factor of 10 (to 5 μl/min), and after about another 2 pore volumes (about 400 hours at this slower flow rate), the experiment reached a second quasi-steady state which then persisted for the remainder of the experiment. However, the precipitation rate of Si and Al at this second steady state was much slower than that measured in the first quasi-steady state (Figure 6B).

This apparent two stage steady state feature was not observed in the KGa-P2 and KGa-P3 experiments. The pump speed was decreased further to 1 μl/min in these two experiments. After being reacted in the flow through reactor for about one and half month (approximately one pore volume), the kaolinite samples in those precipitation experiments eventually showed stable congruent precipitation of Si and Al in the effluent solution, indicating that a steady state had been reached (Figure 7 and 8).

Changes in surface area

The kaolinite sample subjected to the longest combined dissolution and precipitation reaction time was used for BET surface area measurement at the end of the precipitation phase. The measured value was 14.27 m^2/g, which indicated an approximately 20% increase compared to its initial value of 11.8 m^2/g. Grinding effects on the kaolinite surface area are indicated in some flowthrough reactor experiments (METZ and GANOR, 2001), although this effect was minimized in our experiments because of the use of a suspended stir bar. Collision between kaolinite grains and either the stir bar itself or the sides of the reactor still occurred, however, and

this is a likely explanation for the increase, since the mass of newly precipitated material is not enough to account for this increase. Considering the long reaction time of over 7 months this sample had been subjected to and the error in BET measurement (typically about 10%), it was assumed that there was no significant change in sample surface area as a result of reaction. The kinetic data of the sample (KGa-D1) subjected to the longest reaction time was normalized according to its final surface area value. The kinetic rate data of all other samples were all normalized to their initial surface area value before any reaction occurred.

Dissolution and precipitation rates

The dissolution and precipitation rates calculated at steady-state with Equation (3) and the corresponding Gibbs free energy of reaction are shown in Table 4. As expected, the dissolution rates measured far from equilibrium were faster than those measured close to equilibrium. With the exception of the KGa-P1a precipitation experiment, however, the precipitation rates were much slower than the dissolution rates. An early study of Georgia Dry Branch kaolinite at various temperature and pH conditions in which the reactor volume was stirred (GANOR et al., 1995) gave far from equilibrium dissolution rates that agree very well with the values reported in this study. For example, they measured an Al steady state release rate of 1.46×10^{-13} compared to the rate of 1.15×10^{-13} mol/m^2/sec measured in this study at an input pH of 4. The dissolution rate determined here is also broadly consistent with the study of Wieland and Stumm (WIELAND and STUMM, 1992), who determined a rate constant of 2.4×10^{-13} mol/m^2/sec using kaolinite in a batch reactor at pH 4. Using an activation energy of 7.0 kcal/mol and a pH dependence of 0.40 for the kaolinite dissolution reaction (GANOR et al., 1995), the dissolution rates determined in this study were also broadly consistent with those reported in Nagy's study at 80°C and pH 3 using Twiggs country Georgia kaolinite (NAGY et al., 1991). However, with the exception of the KGa-P1a experiment (the initial quasi-steady state rate that could not be maintained), precipitation rates determined in this study were slower than rates determined in Nagy's study (Nagy et al., 1991, 1993) based on an extrapolation from 80°C to 22°C assuming the activation energy for the dissolution reaction applies. The relationship between the rates and reaction free energy is addressed further below.

Solution compositions with respect to potential minerals stabilities

In the kaolinite precipitation experiments, the goal was to keep the input stock solution supersaturated with respect to kaolinite, but undersaturated with respect to gibbsite and all other potential secondary phases. In order to achieve this, it was necessary to use a high Si/Al ratio in the input stock solutions, which resulted in Si concentrations that were in some cases supersaturated with respect to quartz. Since quartz is known to be very difficult to form at room temperature and pressure, precipitation of quartz is considered very unlikely. Other potential secondary phases that might be formed include amorphous silica, gibbsite, imogolite and allophane. The saturation states of these potential mineral phases with respect to the solution compositions at the steady state in the precipitation experiments are shown in Table 5. It is apparent that the steady state solution compositions of precipitation experiments were all undersaturated with respect to those possible aluminum or/and silica-bearing phases. Only the input stock solution for KGa-P3 was slightly supersaturated with respect to gibbsite, imogolite and possibly allophane. Aside from these solubility calculations, it is noteworthy that the Si/Al ratio of 1 at steady state is incompatible with precipitation of either imogolite (Si/Al = 2) or allophane (Si/Al = 1.26 ~ 2). Furthermore, after reaching steady state, the solution composition of KGa-P3 experiment became undersaturated with respect to gibbsite, imogolite and allophane, indicating earlier formation of those phases was very unlikely. For gibbsite, Nagy's dual phase precipitation experiments indicated that precipitation of gibbsite on kaolinite seeds was very unlikely even at these higher temperatures and where the solution was not supersaturated with respect to kaolinite (NAGY and LASAGA, 1993). Since pure kaolinite seed material was used, the stock solution was much more supersaturated with respect to kaolinite and the steady state solution compostions were undersaturated with respect to all other possible aluminum or/and silicon phases, it appears reasonable to assume that kaolinite was the phase formed during the precipitation experiments. Samples in the precipitation experiments were further verified and characterized by Synchrotron X-ray powder diffraction (SXRD) and Scanning Transmission X-ray Microscopy (STXM) techniques.

Characterization of surface precipitates

Synchrotron X-ray diffraction analysis showed no indications of any gibbsite peaks in the samples from the precipitation experiments. However, the mass of newly precipitated materials was very minor, only enough to form a kaolinite layer with a thickness of a few unit cells because of the very slow rates of reaction, despite the fact that precipitation had occurred for over two months. Since the incoming X-ray will penetrate through the sample crystals in a SXRD analysis, however, this technique may not be very sensitive for detecting newly precipitated materials when the total mass of this material is quite small (< 1%).

To further verify that gibbsite did not precipitate, the precipitation samples were also examined by STXM on Beamline 11.0.2 at the Advanced Light Source at Lawrence Berkeley National Laboratory. The STXM beamline has a spatial resolution of 40 nm for sample imaging, but can also perform X-ray absorption spectroscopic analysis of samples. A STXM image of the kaolinite sample from precipitation experiment KGa-P3 is shown in Figure 9A. Under STXM analysis, the kaolinite sample taken from precipitation experiments was not distinguishable morphologically from unreacted kaolinite. In order to verify the phase of the precipitated material formed at the surfaces of seed kaolinite, X-ray absorption spectroscopy was used to compare the Al spectrum of the surface precipitated materials with that of standard kaolinite and gibbsite. X-ray absorption near edge spectra (XANES) is very sensitive to the chemical valence state of an element and its coordination environment within the mineral structure (KONINGSBERGER and PRINS, 1988). It is used as a 'fingerprint' to detect the presence of a particular element and determine its valence, speciation and coordination environment by comparison with the spectra of its standard compounds (HUGGINS et al., 2000; FENTER et al., 2002). In order to examine only the surface layer of the kaolinite sample, spectra were collected under Total Electron Yield (TEY) mode. While the detection limit of the XANES analysis is on the order of 5% (in this regard, greater than the 1% detection limit on a bulk basis that may be achieved with SXRD), the fact that it probes the surface of the crystals makes it a preferred method for determining the identity of newly formed phases, since newly precipitated material is expected to form only on the surfaces of the seed kaolinite, The Al spectrum measured in this way on the surface layer of kaolinite from a precipitation experiment (KGa-P3), as well as kaolinite and gibbsite standards, are shown in Figure 9B. These spectra demonstrate that the Al

spectrum of surface precipitates on seed kaolinite have very similar features to the standard unreacted Georgia kaolinite, while they are significantly different from the gibbsite spectra. While kaolinite has "gibbsite layer" in its basic structure, thus making the overall structure of Al X-ray absorption near edge spectra appear similar for kaolinite and gibbsite, differences between the two minerals due to the presence of silica tetrahedral layers in the kaolinite are still readily apparent (as shown in the circled area on Figure 9B). The similarity between the spectra for standard kaolinite and the surface precipitates indicates the actual formation of kaolinite on the seed materials in the precipitation experiments, in agreement with the prediction based on the thermodynamics of the effluent solution chemistry.

DISCUSSION

Incongruent dissolution

It was shown in Figures 1-3 that all dissolution experiments showed a slight preferential release of Si compared to Al. The possible reasons for this incongruent dissolution include back precipitation of an aluminous phase, re-adsorption of released Al, or dissolution of a silica phase present in the kaolinite samples. Arguing against the role of a silica impurity is the fact that the source clays used in this study were well crystallized pure kaolinite standards from the Clay Mineral Society. In addition, samples used in this study had been washed thoroughly in the pre-treatment procedure. The possibility of silica impurities seems even more unlikely in the case of the KGa-D1 sample, which showed a Si/Al ratio slightly higher than stoichiometric despite extensive dissolution for over 5 months.

The effluent in all of the dissolution experiments remained below saturation with respect to all aluminous phases (gibbsite, boehmite, diaspore) because of the low pH (less than 4.15) and the relatively low Al concentrations. Thus, back precipitation of an aluminous phase appears very unlikely as well.

CARROLL et al. (1988) also reported slightly incongruent dissolution of kaolinite at 25°C between pH 2 and 9 in their long term dissolution experiment. This phenomenon was also observed in the studies of WIELAND and STUMM (1992) at room temperature in far from equilibrium dissolution experiments and was attributed to the adsorption of Al on to the reactive

kaolinite surfaces. Schroth et al. (SCHROTH and SPOSITO, 1997) measured the point of zero net charge to be approximately 3.6 and a permanent structural charge density of -6.3 mmol/kg for of KGa-1 kaolinite, so it appears likely that a small amount of the dissolved Al was re-adsorbed to the kaolinite surface, thus causing the slightly deficiency of Al in the effluent from the reactor.

Evaluation of the effect of dissolved Al on kaolinite dissolution

Oelkers and co-workers reported an Al inhibition effect on silicate mineral dissolution (OELKERS et al., 1994; DEVIDAL et al., 1997). In their studies of kaolinite and albite dissolution at 150°C and 40 bars, the logarithms of the rates at a constant pH showed a linear dependence on aqueous Al concentrations even under far from equilibrium conditions. In this study at 22°C and atmosphere pressure, however, no evidence for Al inhibition was observed. For example, a comparison of dissolution experiments KGa-D3 and KGa-D1b, where the effluent contained 65 and 6.4 μM Al respectively, indicates rates that are the same within experimental uncertainty, or even slightly higher for the higher Al experiment (Table 4). A comparison with all of the other dissolution experiments confirms the lack of an Al effect. The difference in temperature and pressure between the experiments reported here (22°C and 1 bar) and those conducted by Oelkers and co-workers (OELKERS et al., 1994) may explain the difference in the results, although additional systematic experiments over a broader range of pH and Al concentration are needed to further verify this observation at room temperature.

Dependence on Gibbs free energy

Transition State Theory (TST) is a formulation for kinetic rate laws that provides an integral link between the thermodynamic driving force and the rates of kinetic geochemical processes. It has been applied widely in geochemistry to describe the dissolution and crystallization rates of silicates minerals (LASAGA, 1981; AAGAARD and HELGESON, 1982; LASAGA, 1995), with a general form given by (AAGAARD and HELGESON, 1982)

$$R_{net} = R_{+}\left[1 - \exp\left(\frac{-\Delta G}{\sigma RT}\right)\right] \qquad (7)$$

where R_{net} (mol/m^2/sec) is the net overall rate of the reaction (forward rate minus reverse rate), R_+ is the forward (dissolution) reaction rate far from equilibrium per unit surface area mineral, R is the gas constant, T is temperature in degrees Kelvin, σ is Temkin's average stoichiometric number, which is the ratio of the rate of destruction of the activated complex involved in the rate-limiting reaction step with the rate of the overall dissolution rate, and ΔG is the Gibbs free energy (= -A, the chemical affinity) of the overall reaction (kJ/mol or kcal/mol) and is defined in equation (4). The application of Equation (7) assumes that a single rate limiting step controls the overall rate of reaction, that steady-state conditions are met, and that the magnitude of ΔG for each elementary reaction is not much greater than RT.

Using the Gibbs free energy of reaction derived using Equation (4) from the equilibrium constant for kaolinite measured in this study, the kaolinite dissolution and precipitation rates were fitted with Equation (7). The dissolution rate data and the precipitation rate derived from experiment KGa-P1a can be fit very well with Equation (7) using a Temkin coefficient of 2 (Figure 10)

$$R_{diss} = 1.15 \times 10^{-13} \left[1 - \exp\left(\frac{\Delta G}{2RT} \right) \right] \qquad (8)$$

Two distinct regions are apparent in the fit of the dissolutions rates: 1) a far from equilibrium (<-11 kJ/mol or -2.6 Kcal/mol) region where rates are independent of the chemical affinity, and 2) a close to equilibrium (>-11 kJ/mol or -2.6 Kcal/mol) region where the rates depend on the chemical affinity, with the width of this zone determined by the Temkin coefficient. This result is in general agreement with the studies of HUANG (1993) and SOONG and BARNES (1992), who suggested that kaolinite dissolution rates are independent of the saturation index for chemical affinity < about -2 Kcal/mol.

Lasaga and Luttge recently proposed a new step wave dissolution model in which dissolution rates decrease sharply when a critical free energy state corresponding to the opening of etch pits in mineral surface is reached (LASAGA and LUTTGE, 2001; LASAGA and LUTTGE, 2003). However, extending this theory from minerals having relative well developed framework crystal structures (e.g., calcite, feldspar or quartz) to layered silicates is problematic, since dissolution may occur primarily along the edges of the layers (WIELAND and STUMM, 1992; BOSBACH et al., 2000). Given the slow rate of kaolinite dissolution at 25°C, it is a real challenge to measure

rates very close to equilibrium under these conditions, so evaluation of this dissolution mechanism for kaolinite may need to be carried out at higher temperature where the rates are more rapid and *in situ* techniques involving direct microscopic observation can be used. However, we note that Nagy's data at 80°C, which covered a much narrower range of departure from equilibrium (from 0.12 to 0.5 Kcal/mol), showed only a simple linear dependence on the saturation state (NAGY et al., 1991). Evidence collected in this study suggests that the sharp change in dissolution rates predicted by the step wave dissolution model does not occur in the case of kaolinite at room temperature and pressure conditions.

Applying classical crystal growth theory, DOVE et al. (2005) successfully explained the dissolution behavior of quartz, K-feldspar and kaolinite at elevated temperature with two proposed dissolution mechanisms: 1) dissolution at dislocation sites, and 2) dissolution by nucleation of vacancy islands. An attempt was made to interpret the data collected in this study with their proposed models, but neither produced a satisfactory fit. Considering the proposed models were based on quartz dissolution data collected at much higher temperature (200°C), it is suggested that direct extrapolation of these rate models to lower temperature may not be justified.

Precipitation experiment KGa-P1, which had been subjected to over 5 months of dissolution prior to the switch to supersaturated conditions, showed quasi-stable reversible precipitation rates for a period of 4.5 days and is well described by the TST rate law given in Equation (8). This strongly suggests that for short times, precipitation may be fully reversible with respect to dissolution across the range of free energy space investigated up to this point (-23.6 to +4.5 kJ/mol) , although this result may depend on the development of specific reactive sites via extended dissolution. The rapid precipitation rate observed in early quasi-steady state of KGa-P1a sample are most likely related to re-attachment of Si and Al at high energy sites actually created as a result of long-term dissolution far from equilibrium, since similar behavior is not observed for kaolinite seed that were subjected to shorter dissolution times. However, after those active sites originating from the dissolution process were filled, precipitation proceeded by a different, slower growth mechanism.

After the drop in precipitation rate in experiment KGa-P1, and in the case of the other two precipitation experiments KGa-P2 and KGa-P3 that were not subjected to long-term dissolution

in advance, the precipitation rates could not be described adequately with Equation (8). Longer term kaolinite precipitation rates, therefore, are not reversible with the TST dissolution rate law proposed above, implying a change in reaction mechanism between dissolution and long-term, truly steady state precipitation. The precipitation rates data are better described with a linear dependence on the free energy of reaction, ΔG

$$R_{ppt} = 8.0 \times 10^{-15} \left[\frac{\Delta G}{RT} \right] \tag{9}$$

Nagy also obtained a linear relationship between kaolinite precipitation rates and reaction free energy ΔG close to equilibrium at 80 °C and pH 3 (NAGY et al., 1991). The precipitation rates determined by Nagy can be fitted with TST type of rate law, however, with the slopes of the precipitation rates data apparently following the trend of corresponding dissolution rates data within experimental uncertainties. HUANG (1993) and DEVIDAL et al. (1997) determined kaolinite precipitation rates at hydrothermal conditions (between 150 ~ 275 °C, at pH 2, 4.2 and 7.8) and their results also indicate reversible dissolution and precipitation close to equilibrium. The fact that reversibility is not observed in this study across the full range of free energy space considered (-23.6 to +14.8 kJ/mol), except over relatively short times as in experiment KGa-P1a, while it was observed in experiments by NAGY et al. (1991), HUANG (1993), and DEVIDAL et al. (1997) may be the result of the significantly higher temperatures and perhaps the length of the experiment. This highlights one of the difficulties with investigating reaction mechanisms at higher temperature and then extending these via activation energies to lower temperature. There is no guarantee that the same reaction mechanisms will actually apply.

Although Nagy's experiments (NAGY et al., 1991; NAGY and LASAGA,1993) were performed at less than hydrothermal temperatures, the reacting kaolinite had also been pre-equilibrated at 80°C and pH 3 for over 3 months. At hydrothermal conditions or after extensive pretreatment, the surface of kaolinite may be activated, thus resulting in the opening of abundant screw locations and kink sites that could serve as templates for the reversible growth of kaolinite. The applicability of the TST rate law given in Equation (8) during the early quasi-steady state period of experiment KGa-P1, which followed extensive dissolution leaching, is consistent with this interpretation. This study indicates, however, that the steady-state kaolinite rates are not fully

reversible over the entire range of Gibbs free energy investigated, implying that a change in mechanism occurs between dissolution and precipitation. Reversibility of dissolution and precipitation very close to equilibrium, however, is still a possibility.

The kaolinite precipitation experiments in this study covered a range of supersaturation from 4.5 kJ/mol (1.0 kcal/mol) to 14.8 kJ/mol (3.6 kcal/mol). Despite this relatively large range of supersaturation, the precipitation experiments showed a linear dependence on free energy. Although a detailed precipitation rate mechanism is not possible without further microscopic and/or spectroscopic characterization of the newly precipitated kaolinite, it is worth discussing some of the possible growth mechanisms that might apply under these experimental conditions. Crystal growth models have been reviewed extensively in the literature (BENNEMA and GILMER, 1973; OHARA and REID, 1973; NIELSEN, 1984) and are generally classified as diffusion controlled, or surface integration controlled, or both. Only surface integration growth models will be considered for the precipitation experiments conducted in this study, since kaolinite growth at room temperature is very slow and unlikely to be diffusion controlled. The surface-controlled mechanisms consist of adsorption of lattice ions, spiral growth at screw dislocations, or two-dimensional nucleation on the mineral surface. In the case of two-dimensional nucleation, growth proceeds by the addition of nuclei similar to the template on which they form or through the attachment of growth units to the edge of the nuclei via surface diffusion. A number of two-dimensional nucleation growth models have been proposed in the literature and can be classified into mononuclear or polynuclear mechanisms (OHARA and REID, 1973; NIELSEN, 1984). The main differences between these models are in their assumptions about the rate of surface nucleation and the rate of lateral spreading of the nuclei across the crystal surface. The two-dimensional nucleation growth models can be expressed as (LI et al., 2003)

$$R = k_{sn} F(\Omega - 1) \exp\left(-\frac{\phi^2}{(kT)^2} \frac{1}{\ln(\Omega)} \right), \qquad (10)$$

where k_{sn} is the rate constant for mononuclear or polynuclear growth, Ω is the relative supersaturation ratio (Equation 4), $F(\Omega)$ is a function of supersaturation, ϕ is defined as the edge free energy (in kJ mol^{-1}) and k is the Boltzmann constant.

Such two dimensional nucleation growth models have been discussed extensively in the case of gibbsite crystal growth that occurs in the industrial Bayer process (FARHADI and BABAHEIDARY, 2002; LI et al., 2003; VEESLER and BOISTELLE, 1994). Gibbsite has an analogous structure to that of the micas and the neutral aluminum hydroxide sheets are typically found to be sandwiched between silicate sheets in important clay groups, such as the kaolinite, illite, and montmorillonite/smectite. In kaolinite, the individual aluminum hydroxide layers are identical to the individual layers of gibbsite (referred to as the "gibbsite layers") and therefore may provide some guidance for possible interpretations of kaolinite precipitation kinetics. Following the simplified mononuclear equation proposed by BOTSARIS and DENK (1970) to describe the formation and spreading of two-dimensional nuclei during gibbsite growth, Equation (10) can be simplified as

$$R = k_{sn} \exp\left(-\frac{\phi^2}{(kT)^2} \frac{1}{\ln(\Omega)} \right). \tag{11}$$

According to the this simplified equation (which assumes the pre-exponential term depending on the Gibbs free energy is equal to 1), the logarithm of the kaolinite precipitation rates will show a linear trend against the term $1/\left(T^2 \ln \Omega\right)$ if the two dimensional nucleation growth model applies (Figure 11). When plotted in this way, the data show a high degree of linearity between those two parameters (with a R^2 of 0.986), indicating the two-dimensional nucleation model is at least compatible with the precipitation rates determined in this study. The free edge energy determined using the slope of linear regression fitting line from Figure 11 is 3.54 kJ/mol, which is comparable to the value obtained for gibbsite at 55 °C (from 2.6 to 6.0 kJ/mol as reported in the study of FARHADI and BABAHEIDARY [2002]), further supporting the applicability of the model for kaolinite crystal growth presented above.

Kaolinite precipitation rates and their effect on mineral weathering rates

It has been suggested that clay precipitation rates may influence or even control the weathering rates of primary phases like the feldspars (ALEKSEYEV et al., 1997; ZHU et al., 2004; MAHER et al., 2006). A comprehensive investigation of this question is beyond the scope of the present study, and is not possible in any case at this point because the dependence of kaolinite

precipitation rates on pH has not yet been determined. However, it is instructive to consider whether the kaolinite precipitation rate determined in this study at pH 4 is rapid enough to keep up with feldspar dissolution rates, thus maintaining the pore water close to equilibrium with respect to kaolinite. If kaolinite precipitation rates are pH dependent, what kind of decrease would be necessary to result in significant supersaturation with respect to kaolinite? To answer these questions, we consider a set of idealized reactive transport simulations of the chemical weathering of plagioclase feldspar (albite) to kaolinite at 25ºC using the rate law proposed by HELLMANN and TISSERAND (2006) for albite and the kaolinite precipitation rates determined in this study. The albite dissolution rate constant, which HELLMANN and TISSERAND (2006) determined at 150ºC as a function of ΔG, was adjusted to 25ºC using an activation energy of 62.7 kJ/mol. Additionally, the rate constant was decreased by 0.75 log units (in units of mol/m^2/s) so as to represent a dissolution rate in the circumneutral pH range. Following the formulation proposed by HELLMANN and TISSERAND (2006), this yielded two parallel rate laws at 25ºC (in units of mol/m^2/s)

$$R_1 = 1.02 \times 10^{-12} \left\{ 1 - \exp\left[-0.0000798 \left(\left| \frac{\mathrm{Ln}\Omega}{RT} \right| \right)^{3.81} \right] \right\} \tag{12}$$

$$R_2 = 1.81 \times 10^{-14} \left\{ 1 - \exp\left[-\left| \frac{\mathrm{Ln}\Omega}{RT} \right| \right] \right\}^{1.17} \tag{13}$$

For kaolinite, the form of the rate law presented in Equation (11) was used. A reactive transport calculation using the code *CrunchFlow* (STEEFEL, 2007) was carried out for conditions broadly similar to those investigated by WHITE et al (in press) at the Santa Cruz chronosequences. A flow rate of 0.088 m/yr, volume fractions of albite and kaolinite of 15% and 10% respectively, and specific surface areas of 0.43 m^2/g and 11.83 m^2/g for albite and kaolinite respectively were assumed for the calculations, which were then carried out to 65,000 years (the approximate age of the youngest terrace at Santa Cruz). In the calculation, a modified rainwater with a pH of 5.73 infiltrates the sandy material (porosity = 40%) under partially saturated conditions.

Using the kaolinite precipitation rate determined in this study at pH 4 along with the rate law for albite proposed by HELLMANN and TISSERAND (2006), the reactive transport calculations

predict that the pore water composition will remain close to equilibrium with respect to kaolinite (log Q/Keq ~ 0.1), while albite remains far from equilibrium (Figure 12). However, the results at circumneutral pH (6-8) depend critically on the pH dependence of kaolinite precipitation rates. If the pH dependence is significant (e.g., a dependence ≥ 1), then the decrease in the kaolinite precipitation rate as the pH increases could have marked effect on the weathering rate of albite. This can be evaluated by simulating the same system using slower rates for kaolinite precipitation. As the kaolinite precipitation rate constant decreases from 10^{-15} mol/m^2/s (log k = -15) to 10^{-16} mol/m^2/s (log k = -16), the simulations predict that the kaolinite supersaturation will rise substantially, while the feldspar approaches equilibrium more closely (Figure 12). While these are idealized simulations intended to explore the coupling between feldspar dissolution and kaolinite precipitation rates, they demonstrate that clay precipitation rates could influence or even control the overall rate at which chemical weathering occurs if the rates are pH dependent. The simulations also highlight the need for additional experiments to determine the pH dependence of kaolinite precipitation rates.

SUMMARY AND CONCLUSIONS

Kinetic rates of kaolinite dissolution and precipitation at room temperature and pressure were measured at pH values close to 4 as a function of Gibbs free energy using well crystallized low defect Georgia kaolinite. Dissolution rates measured close to equilibrium (generally within about 2 kcal/mol) showed an exponential decrease compared to far from equilibrium rates. This observed trend can be described well within the framework of Transition State Theory with a Temkin coefficient of 2, implying that the activated complexes involved in the rate-limiting step for kaolinite dissolution involved either a single Al or Si atom. Dissolution with input solutions having high Al concentration showed no evidence for significant Al inhibition at the experimental conditions considered in this study.

Long-term precipitation rates at 22°C and close to pH 4 are much slower than the dissolution rates and generally fall off the trend predicted by Transition State Theory. Only a kaolinite sample that was subjected to extensive dissolution for over 5 months under far from equilibrium conditions showed a faster precipitation rate for an initial quasi-steady state that is compatible with the TST model. The fact that this reversible precipitation stage lasted only about 110 hours,

at which point precipitation rates decreased by an order of magnitude, suggests that activated sites created during the long-term, far from equilibrium dissolution process became filled and a different growth mechanism ensued. The other two precipitation experiments performed under more supersaturated conditions and with kaolinite seed that had not undergone extensive dissolution far from equilibrium, also showed very slow precipitation rates that are not compatible with a reversible TST rate law based on dissolution rates. The long-term precipitation rates show instead a linear dependence on the Gibbs free energy, with the relationship between the rates and corresponding reaction free energies described satisfactorily with a simplified two dimensional nucleation growth model.

A set of idealized reactive transport simulations of the transformation of plagioclase feldspar (albite) to kaolinite was used to demonstrate that the rate of kaolinite precipitation, and in particular its as yet undetermined pH dependence, could influence or even control the overall rate at which chemical weathering occurs.

Acknowledgements

The authors thank Tolek Tyliszczak, Simon Teat and Matthew Marcus at the Advanced Light Source of Lawrence Berkeley National lab for their help on synchrotron STXM and XRD analysis. We would also like to thank Kathryn Nagy, Jiwchar Ganor, Patrick Brady, and Susan Carroll for their constructive reviews that substantially improved this manuscript. The Advanced Light Source is supported by the Director, Office of Science, Office of Basic Energy Sciences, of the U.S. Department of Energy under Contract No. DE-AC02-05CH11231. This work was supported by the Director, Office of Science, Office of Basic Energy Sciences, Division of Chemical Sciences, Geosciences, and Biosciences of the U.S. Department of Energy under Contract No. DE-AC02-05CH11231 to Lawrence Berkeley National Laboratory.

REFERENCES CITED

Aagaard P. and Helgeson H. C. (1982) Thermodynamic and kinetic constraints on reaction rates among minerals and aqueous solutions, I. Theoretical considerations. *American Journal of Science* **282**, 237-285.

Abbate M., J. B. Goedkoop J. B., de Groot F. M. F., M. Grioni M., Fuggle J. C., Hofmann S., Petersen H., and Sacchi M. (1992) Probing depth of soft x-ray absorption spectroscopy measured in total-electron-yield mode. *Surface and Interface Analysis* **18**(1), 65-69.

Alekseyev V. A., Medvedeva L. S., Prisyagina N. I., Meshalkin S. S., and Balabin A. I. (1997) Change in the dissolution rates of alkali feldspars as a result of secondary mineral precipitation and approach to equilibrium. *Geochimica Cosmochimica Acta* **61**(6), 1125-1142.

Bennema P., and Gilmer G. H. (1973). In *Crystal growth: An Introduction*, Ed. Hartman P, (North-Holland Amsterdam), 263.

Bosbach D., Charlet L., Bickmore B., and Hochella M. F. (2000) The dissolution of hectorite: In-situ, real-time observations using atomic force microscopy. *American Mineralogist* **85**(9), 1209-1216.

Botsaris G. D. and Denk E. G. (1970) Growth Rates of Aluminum Potassium Sulfate Crystals in Aqueous Solutions. *Ind. Eng. Chem. Fund.* **9**(2), 276-283.

Cama J., Metz V., and Ganor J. (2002) The effect of pH and temperature on kaolinite dissolution rate under acidic conditions. *Geochimica Et Cosmochimica Acta* **66**(22), 3913-3926.

Cama, J. and Ganor, J. (2006). The effects of organic acids on the dissolution of silicate minerals: A case study of oxalate catalysis of kaolinite dissolution. *Geochim. Cosmochim. Acta* **70**, 2191-2209.

Carroll-Webb S. A. and Walther J. V. (1988) A surface complex reaction model for the pH-dependence of corundum and kaolinite dissolution rates. *Geochimica et Cosmochimica Acta* **52**(11), 2609-2623.

Carroll S. A. and Walther J. V. (1990) Kaolinite dissolution at 25°C , 50°C , and 80°C *American Journal of Science* **290**(7), 797-810.

Devidal J. L., Schott J., and Dandurand J. L. (1997) An experimental study of kaolinite dissolution and precipitation kinetics as a function of chemical affinity and solution composition at 150 degrees C, 40 bars, and pH 2, 6.8, and 7.8. *Geochimica Cosmochimica Acta* **61**(4), 5165-5186.

Dove P. M., Han N., and De Yoreo J. J. (2005) Mechanisms of classical crystal growth theory explain quartz and silicate dissolution behavior. *PNAS* **102**(43), 15357-15362.

Ebel H., Mantler M., Svagera R., and Kaitna R. (1994) Investigation of thin films by soft X-ray fluorescence and by total electron yield measurements. *Surface and Interface Analysis* **22**(1-12), 602-604.

Farhadi F. and Babaheidary M. B. (2002) Mechanism and estimation of Al(OH)3 crystal growth. *Journal of Crystal Growth* **234**(4), 721-730.

Fenter P.A., Rivers, M.L., Sturchio, N.C., Sutton, S.R. (Eds.), (2002) Application of synchrotron radiation in low-temperature geochemistry and environmental science. *Reviews in Mineralogy & Geochemistry*, Vol. **49**, Mineralogical Society of America, Washington.

Ganor J., Mogollon J. L., and Lasaga A. C. (1995) The effect of pH on kaolinite dissolution rates and on activation energy. *Geochimica et Cosmochimica Acta* **59**(6), 1037-1052.

Hellmann R. and Tisserand D. (2006) Dissolution kinetics as a function of the Gibbs free energy of reaction: An experimental study based on albite feldspar. *Geochimica et Cosmochimica Acta* **70**(2), 1037-1052.

Huang W.-L. (1993) Stability and kinetics of kaolinite to boehmite conversion under hydrothermal conditions. *Chemical Geology* **105**(1-3), 197-214.

Huertas F. J., Chou L., and Wollast R. (1999) Mechanism of kaolinite dissolution at room temperature and pressure Part II: kinetic study. *Geochimica et Cosmochimica Acta* **63**(19-20), 3261-3275.

Huggins F.E., Huffman, G.P., Robertson, J.D. (2000) Speciation of elements in NIST particulate matter SRMs 1648 and 1650, *J. Hazard. Mater.* **74**, 1-23.

Koningsberger, D.C., Prins, R. (1988) X-ray Absorption: principles, applications, techniques of EXAFS, SEXAFS and XANES. New York, Wiley.

Lasaga A. C. (1981) Rate laws in chemical reactions. In *Kinetics of Geochemical Processes*, Vol. 8 (ed. A. C. L. a. R. J. Kirkpatrick), pp. 135-169. Mineralogical Society of America.

Lasaga A. C. (1995) Fundamental approaches in describing mineral dissolution and precipitation rates. In *Chemical Weathering Rates of Silicate Minerals*, Vol. 31, pp. 23-86.

Lasaga A. C. and Luttge A. (2001) Variation of crystal dissolution rate based on a dissolution stepwave model. *Science* **291**(5512), 2400-2404.

Lasaga A. C. and Luttge A. (2003) A model for crystal dissolution. *European Journal of Mineralogy* **15**(4), 603-615.

Li T. S., Livk I., and Ilievski D. (2003) Supersaturation and temperature dependency of gibbsite growth in laminar and turbulent flows. *Journal of Crystal Growth* **258**(3-4), 409-419.

Maher K., Steefel C. I., DePaolo D. J., and Viani B. E. (2006) The mineral dissolution rate conundrum: Insights from reactive transport modeling of U isotopes and pore fluid chemistry in marine sediments. *Geochimica Et Cosmochimica Acta* **70**(2), 337-363.

May H. M., Helmke, P. A., and Jackson, M. L. (1979) Gibbsite solubility and thermodynamic properties of hydroxyaluminum ions in aqueous solution at 25 °C. Geochim. Cosmochim. Acta 43(6), 861-868.

May H. M., Kinniburgh D. G., Helmke P. A., and Jackson M. L. (1986) Aqueous Dissolution, Solubilities and Thermodynamic Stabilities of Common Aluminosilicate Clay-Minerals - Kaolinite and Smectites. *Geochimica Et Cosmochimica Acta* **50**(8), 1667-1677.

Metz V. and Ganor J. (2001) Stirring effect on kaolinite dissolution rate. *Geochimica et Cosmochimica Acta* **65**(20), 3475-3490.

Miller J. C. and Miller J. N. (1993) *Statistics for Analytical Chemistry*. Ellis Horwood.

Nagy K. L., Steefel, C. I., Blum, A. E., and Lasaga, A. C., 1990. Dissolution and precipitation kinetics of kaolinite: initial results at 80°C with application to porosity evolution in a sandstone. In: Meshri, I. D. and Ortoleva, P. J. Eds.), Prediction of Reservoir Quality Through Chemical Modeling.

Nagy K. L., Blum A. E., and Lasaga A. C. (1991) Dissolution and precipitation kinetics of kaolinite at 80°C and pH 3 - the dependence on solution saturation state. *American Journal of Science* **291**(7), 649-686.

Nagy K. L. and Lasaga A. C. (1993) Simultaneous precipitation kinetics of kaolinite and gibbsite at 80°C and pH 3. *Geochimica et Cosmochimica Acta* **57**(17), 4329-4335.

Nielsen A. E. (1984) Electrolyte crystal growth mechanisms. *Journal of Crystal Growth* **67**(2), 289-310.

Oelkers E. H., Schott J., and Devidal J.-L. (1994) The effect of aluminum, pH, and chemical affinity on the rates of aluminosilicate dissolution reactions. *Geochimica et Cosmochimica Acta* **58**(9), 2011-2024.

Ohara M. and Reid R.C. (1973) *Modelling Crystal Growth rates from Solutions*. Prentice-Hall, Englewood Cliffs, NJ.

Parkhurst D. L. and Appelo C. A. J. (1999) User's guide to PHREEQC (version 2)--A computer program for speciation, batch-reaction, one-dimensional transport, and inverse geochemical calculations. In *U.S. Geological Survey Water-Resources Investigations Report*, pp. 312. U.S. Geological Survey.

Schroth B. K. and Sposito G. (1997) Surface charge properties of kaolinite. *Clays and Clay Minerals* **45**(1), 85-91.

Soong C. and Barnes H. L. (1992) Precipitation and dissolution kinetics of kaolinite under hydrothermal conditions. *Geological Society of America, Abstracts with Programs* **24**, 7.

Steefel, C. I. (2007) User's Guide to CrunchFlow. Lawrence Berkeley National Laboratory Report.

Steefel C. I. and Van Cappellen P. (1990) A new kinetic approach to modeling water-rock interaction: the role of nucleation, precursors, and Ostwald ripening. *Geochimica et Cosmochimica Acta* **54**(10), 2657-2677.

Su C. and Harsh J. B. (1998) Dissolution of allophone as a thermodynamically unstable solid in the presence of boehmite at elevated temperatures and equilibrium vapor pressures. *Soil Sci.* **163**(4), 299-312.

Veesler S. and Boistelle R. (1994) Growth kinetics of hydrargillite $Al(OH)_3$ from caustic soda solutions. *Journal of Crystal Growth* **142**(1-2), 177-183.

Wieland E. and Stumm W. (1992) Dissolution kinetics of kaolinite in acidic aqueous solutions at 25°C *Geochimica Et Cosmochimica Acta* **56**(9), 3339-3355.

White A.F., Schulz M.S., Vivit D.V., Blum A.E., Stonestrom D.A., Anderson S.P. (in press), Chemical weathering of a marine terrace chronosequence, Santa Cruz, California I:

Deciphering reaction rates from element and mineral depth profiles. *Geochimica et Cosmochimica Acta.*

Xie, Z. and Walther, J. V., 1992. Incongruent dissolution and surface area of kaolinite. Geochim. Cosmochim. Acta 56, 3357-3363.

Zhu C., Blum A. E., and Veblen D. (2004) Feldspar dissolution rates and clay precipitation in the Navajo aquifer at Black Mesa, Arizona, USA. *Proceedings of the 11th International Symposium on Water-Rock Interaction,* R.B. Wanty and R.R. Seal (eds.), Taylor and Francis Group, London, 895-899.

TABLES

Table 1: Al and Si species and their hydrolysis constants used in speciation calculation*.

Reaction	$\log K_{eq}$
$Al^{+3} + H_2O = AlOH^{+2} + H^+$	-5.00
$Al^{+3} + 2H_2O = Al(OH)^{2+} + 2H^+$	-10.1
$Al^{+3} + 3H_2O = Al(OH)^0_3 + 3H^+$	-16.9
$Al^{+3} + 4H_2O = Al(OH)^{4-} + 4H^+$	-22.7
$H_4SiO_4 = H_3SiO_4^- + H^+$	-9.83

*from PHREEQC (PARKHURST and APPLEO, 1999) database.

Table 2: Target input Si and Al concentrations

Experiment	Si (μM)	Al (μM)
Dissolution		
1	0	0
2	300	0
3	0	60
Precipitation		
4	500	100
5	1000	100
6	1500	200

Table 3: Al and Si concentration in solutions equilibrated with kaolinite for determination of its solubility constant*

Label	pH	Si (μM)	Al (μM)	$\log(a_{H4SiO4})$	$\log(a_{Al3+})$	log(IAP)
Sample 1	4.22	311.98±3.06	11.42±0.44	-3.505	-5.336	7.638
Sample 2	4.20	312.94±2.47	11.27±0.37	-3.504	-5.340	7.512

*Average result from this two sampling points were used to calculate the equilibrium solubility of kaolinite sample used in this study

Table 4: Summary of experimental conditions and results

Sample label	Starting material (g)	Pump speed (ml/min)	Input pH	Input Si (μM)	Input Al (μM)	Output Si (μM)	Output Al (μM)	Output pH	Rate from Al (mol/m^2/sec)	Saturation index	ΔG (kJ/mol)
KGa-D1a	2.000	0.050	4.001	0.00	0.00	9.84 (±0.14)	7.88 (±0.10)	4.076	-1.15 (±0.06) E-13	-4.17	-23.56(±0.80)
KGa-D1b	2.000	0.050	3.987	277.33 (±0.97)	0.00	287.72 (±3.18)	6.43 (±0.10)	4.033	-9.37(±0.14) E-14	-1.66	-9.38(±0.80)
KGa-D2a	1.000	0.041	4.004	277.63 (±3.33)	0.21 (±0.04)	288.83 (±3.50)	3.76 (±0.09)	4.049	-1.04(±0.06) E-13	-2.03	-11.47(±0.73)
KGa-D2b	1.000	0.012	4.004	277.63 (±3.33)	0.21 (±0.04)	295.95 (±4.58)	8.45 (±0.14)	4.102	-6.77(±0.36) E-14	-1.00	-5.65(±0.85)
KGa-D3	1.000	0.049	4.016	0.26 (±0.04)	60.5 (±0.58)	6.59 (±0.09)	65.21 (±0.80)	4.038	-1.46 (±0.76) E-13	-2.91	-16.44(±0.80)
KGa-P1a	2.000	0.050	4.080	493.49 (±4.24)	106.25 (±1.10)	478.82 (±4.35)	96.09 (±1.17)	3.980	1.47 (±0.24) E-13	0.80	4.52(±0.73)
KGa-P1b	2.000	0.005	4.022	498.03 (±6.39)	113.49 (±1.68)	494.89 (±3.40)	106.02 (±0.89)	3.964	1.04 (±0.27) E-14	0.82	4.63(±0.73)
KGa-P2	1.000	0.001	4.135	1030.96 (±29.67)	118.78 (±3.32)	1008.11 (±6.40)	96.27 (±0.56)	3.950	1.64 (±0.35) E-14	1.34	7.57(±0.73)
KGa-P3	1.000	0.001	4.270	1466.85 (±27.80)	242.18 (±4.76)	1412.23 (±20.68)	210.09 (±6.26)	4.006	2.50(±0.74) E-14	2.63	14.85(±0.85)

Table 5. Steady state saturation indices for potential secondary phases in precipitation experiments.

	Saturation Index						
	Kaolinite[1]	Allophane[2]	Imogolite[2]	Gibbsite[3]	Amorphous silica[4]	Halloysite[5]	Quartz[4]
KGa-P1a	0.87	-2.441	-1.841	-0.741	-0.579	-2.84	0.711
KGa-P1b	0.888	-2.438	-1.838	-0.747	-0.564	-2.822	0.726
KGa-P2	1.342	-2.293	-1.693	-0.829	-0.255	-2.368	1.035
KGa-P3	2.662	-1.125	-0.525	-0.321	-0.103	-1.048	1.187

[1] Kaolinite equilibrium solubility constant was from current study; [2] Allophane and imogolite equilibrium solubility constants were taken from SU and HARSH (1998); [3.] Gibbsite equilibrium solubility constant was from MAY et al. (1979); [4] Amorphous silica and quartz equilibrium solubility constants were taken from PHREEQC database (PARKHURST and APPELO, 1999); [5] Halloysite solubility data was from HEM et al. (1973).

FIGURE CAPTIONS

Figure 1: Effluent ΔC_{Al} and ΔC_{Si} variation in KGa-D1 dissolution experiments at pH 4, 22 °C with input solutions having (KGa-D1a) no Si and Al (solid symbol) and (KGa-D1b) 500 μM Si and no Al (open symbol). Pumping speed: 0.05 mL/min.

Figure 2: Effluent ΔC_{Al} and ΔC_{Si} variations in KGa-D2 dissolution experiments at pH 4, 22 °C with input solution having 500μM Si and no Al; (KGa-D2a) pump speed: 0.05ml/min (solid symbol) and (KGa-D2b) pump speed: 0.01ml/min (open symbol).

Figure 3: Effluent ΔC_{Al} and ΔC_{Si} variations in KGa-D3 dissolution experiments at pH 4, 22 °C with input solution having 60 μM Al and no Si; pump speed: 0.05ml/min.

Figure 4: Steady state effluent ΔC_{Al} versus ΔC_{H^+} in the kaolinite dissolution/precipitation experiments at pH 4, 22 °C with varying input solution composition and pumping speed. Dashed line represents the ideal theoretical stoichiometric slope of 3.

Figure 5: Steady state effluent ΔC_{Al} versus ΔC_{Si} in the kaolinite dissolution/precipitation experiments at pH 4, 22 °C with varying input solution composition and pumping speed. The smaller graph inside the larger one shows an expanded view of the data for the KGa-D1a experiment. Dashed line represents the ideal theoretical stoichiometric slope of 1.

Figure 6: Effluent ΔC_{Al} and ΔC_{Si} variations in the KGa-P1 precipitation experiment at pH 4, 22 °C with input solution having 0.5mM Si and 0.1mM Al; (A)pump speed: 0.05ml/min (solid symbol) and (B) pump speed: 0.005ml/min (open symbol).

Figure 7: Effluent ΔC_{Al} and ΔC_{Si} variations in the KGa-P2 precipitation experiment at pH 4, 22 °C with input solution having 1mM Si and 0.1mM Al; pump speed: 0.001ml/min.

Figure 8: Effluent ΔAl and ΔSi concentration variations in the KGa-P3 precipitation experiment at pH 4, 22 °C with input solution having 1.5mM Si and 0.2mM Al; pump speed: 0.001ml/min.

Figure 9: A) STXM image of kaolinite samples in precipitation experiments. B). Al XANES spectra of kaolinite particles by total electron yield mode in precipitation experiments by STXM (circled area highlights the major difference between the spectra).

Figure 10: Kaolinite dissolution/precipitation rate vs. reaction free energy at pH 4, 22 °C; the blue dashed line (a) was fitted with TST theory and the red dashed line (b) was fitted with two dimensional nucleation model (for details, see the text for further discussion).

Figure 11: Linear fitting of kaolinite precipitation rate data with a mononuclear two dimensional nucleation growth model at the experimental temperature of 22 °C.

Figure 12: Reactive transport simulations of pore water kaolinite and albite saturation indices ($\text{Log } Q/K_{eq}$) versus depth for a chemical weathering profile infiltrated by a solution at pH 5.73. If the kaolinite precipitation rate is independent of pH and the rate determined in this study at pH 4 is used directly, then the simulations predict that the pore waters will remain close to equilibrium with respect to kaolinite. If a relatively strong pH dependence exists ($n \geq 1$), then significant supersaturation with respect to kaolinite may occur due to the decrease in the rate constant with increasing pH. “Log k” in the figure refers to the logarithm of the rate constant assumed for kaolinite precipitation ($\text{mol/m}^2\text{/s}$) following the formulation in Equation (11).

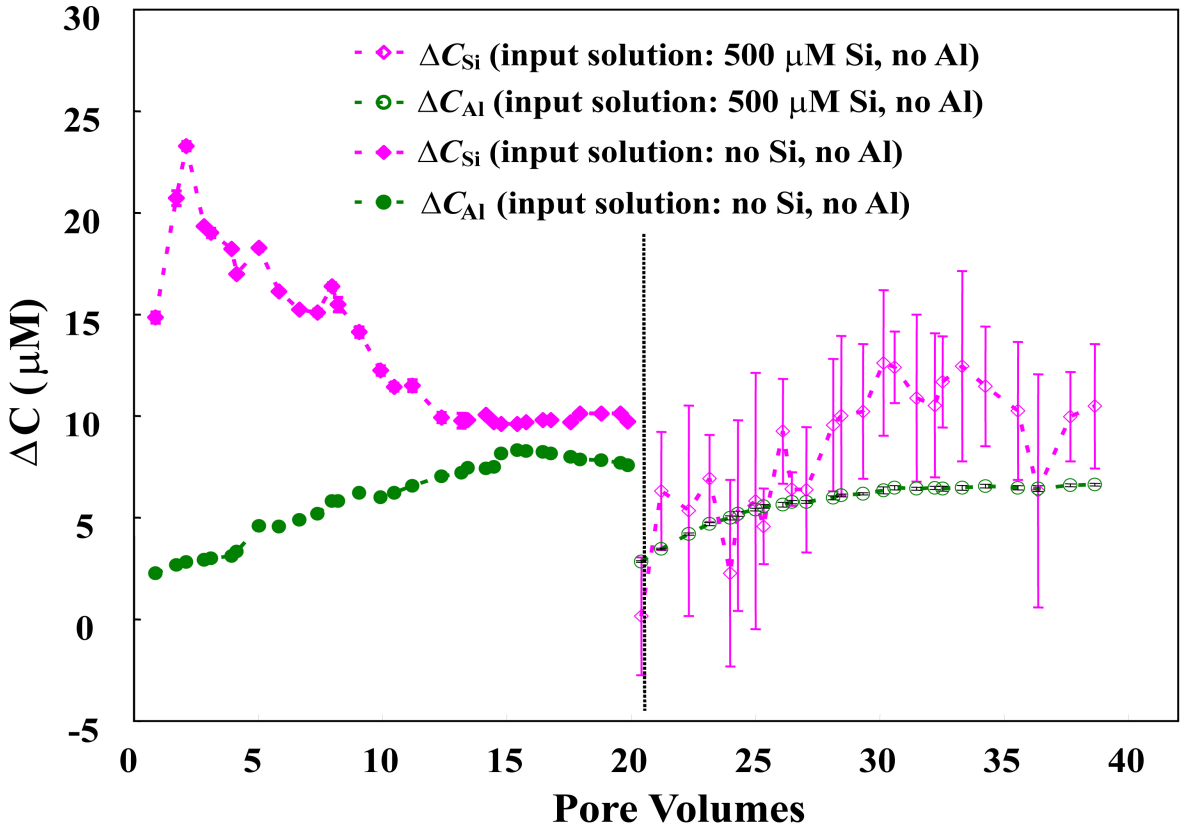
30
25
20
15
10
5
0
-5
ΔC (μM)
0
5
10
15
20
25
30
35
40
Pore Volumes
ΔCSi (input solution: 500 μM Si, no Al)
ΔCAl (input solution: 500 μM Si, no Al)
ΔCSi (input solution: no Si, no Al)
ΔCAl (input solution: no Si, no Al)

Figure 1

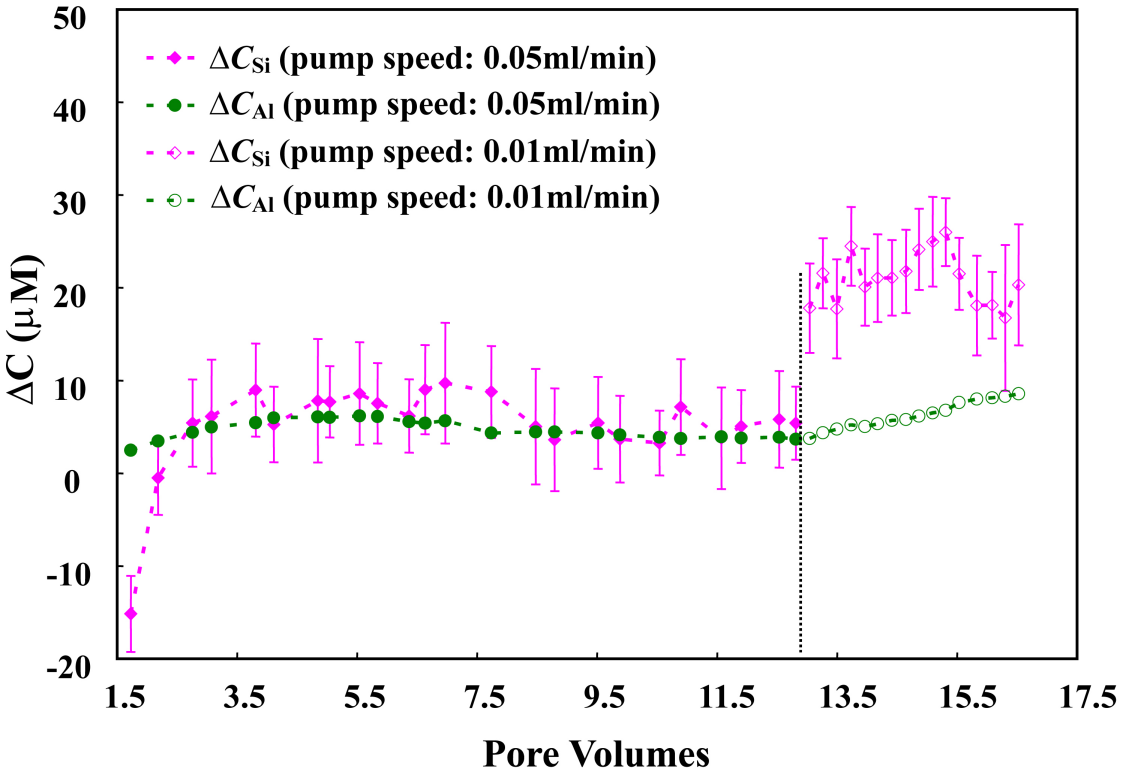
50
40
30
20
10
0
-10
-20
ΔC (μM)
1.5
3.5
5.5
7.5
9.5
11.5
13.5
15.5
17.5
Pore Volumes
ΔCSi (pump speed: 0.05ml/min)
ΔCAl (pump speed: 0.05ml/min)
ΔCSi (pump speed: 0.01ml/min)
ΔCAl (pump speed: 0.01ml/min)

Figure 2

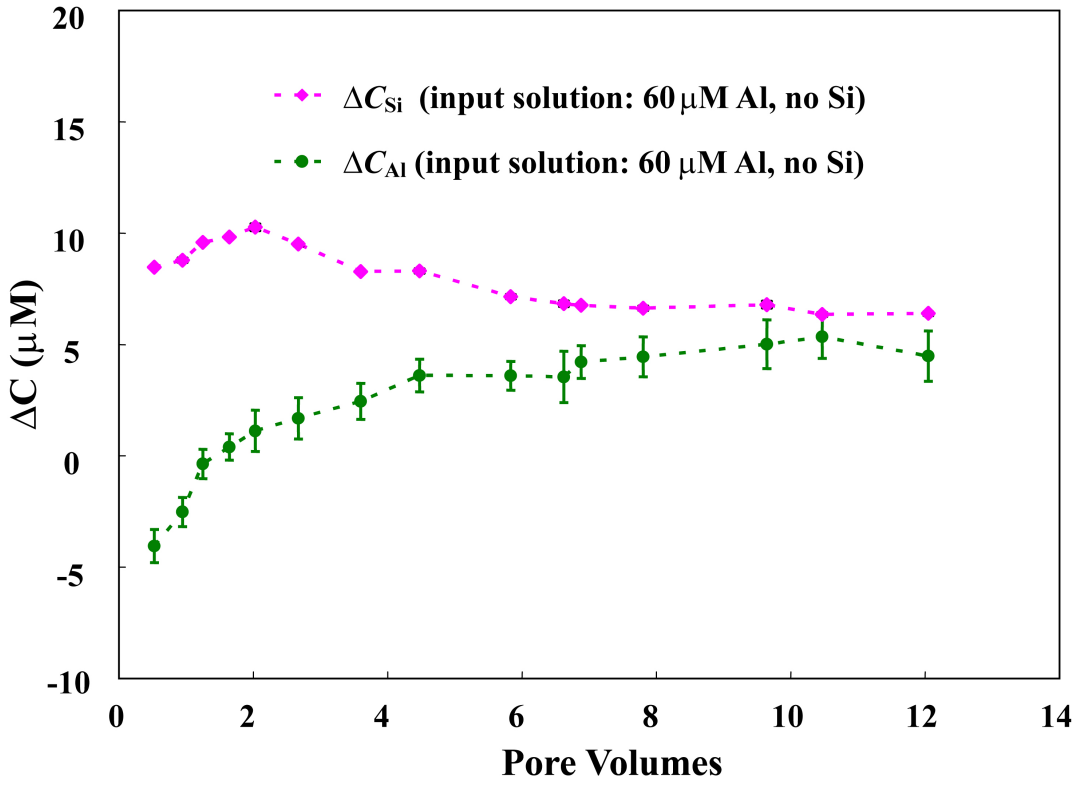
20
15
10
5
0
-5
-10
ΔC (μM)
0
2
4
6
8
10
12
14
Pore Volumes
ΔCSi (input solution: 60 μM Al, no Si)
ΔCAl (input solution: 60 μM Al, no Si)

Figure 3

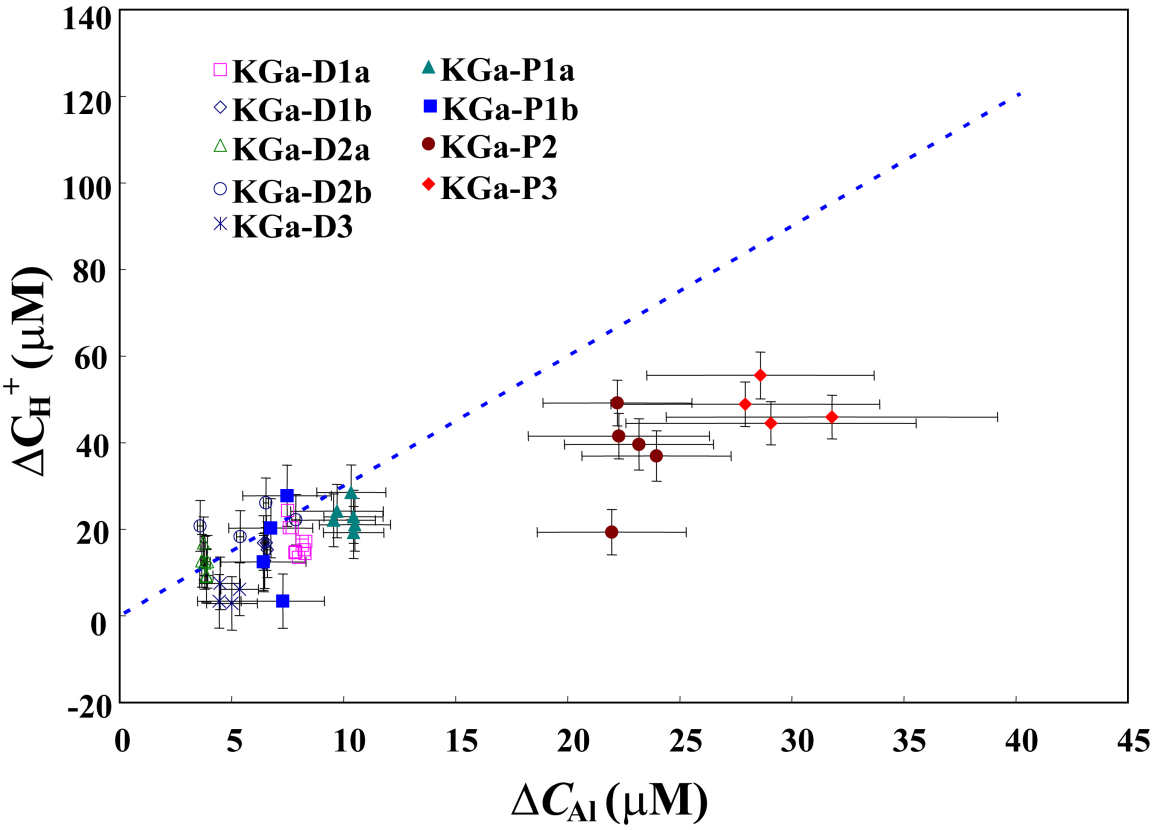
KGa-D1a
KGa-D1b
KGa-D2a
KGa-D2b
KGa-D3
KGa-P1a
KGa-P1b
KGa-P2
KGa-P3
ΔC_H+ (μM)
ΔC_Al (μM)
140
120
100
80
60
40
20
0
-20
0
5
10
15
20
25
30
35
40
45

Figure 4

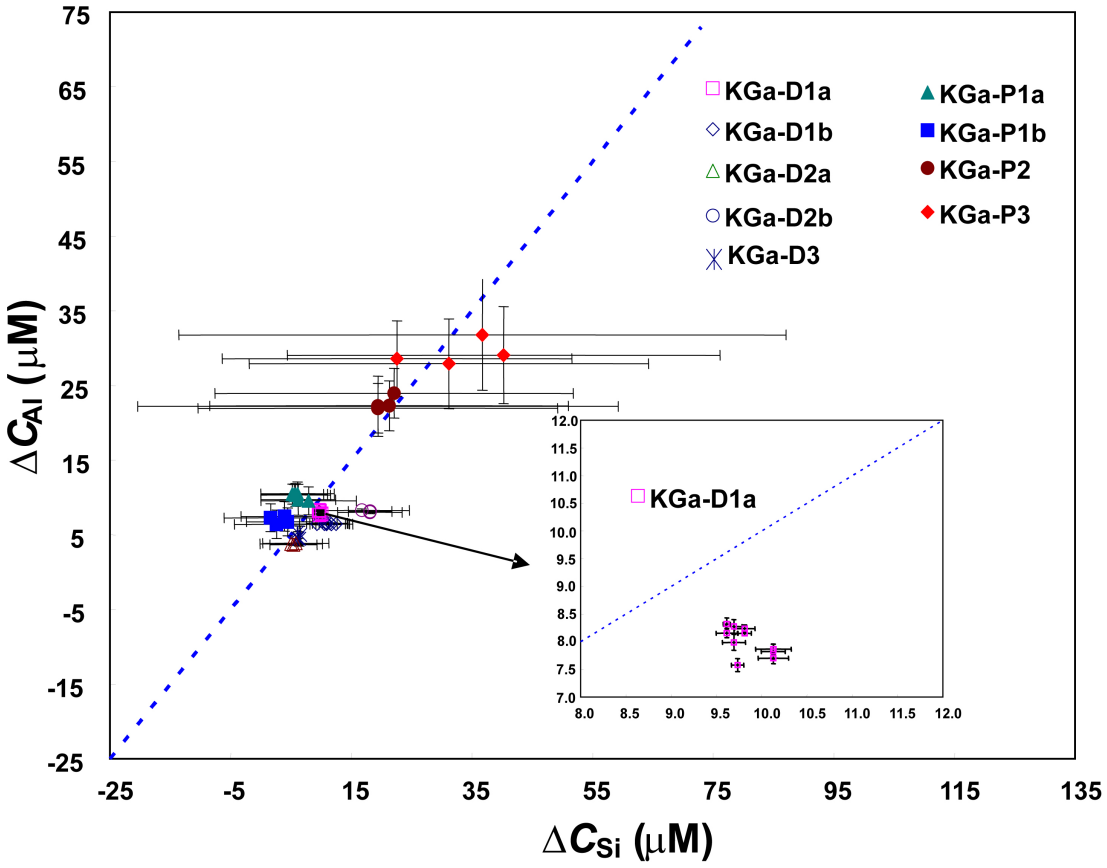
KGa-D1a
KGa-D1b
KGa-D2a
KGa-D2b
KGa-D3
KGa-P1a
KGa-P1b
KGa-P2
KGa-P3
ΔCAl (μM)
ΔCSi (μM)
75
65
55
45
35
25
15
5
-5
-15
-25
-25
-5
15
35
55
75
95
115
135
12.0
11.5
11.0
10.5
10.0
9.5
9.0
8.5
8.0
7.5
7.0
8.0
8.5
9.0
9.5
10.0
10.5
11.0
11.5
12.0
KGa-D1a

Figure 5

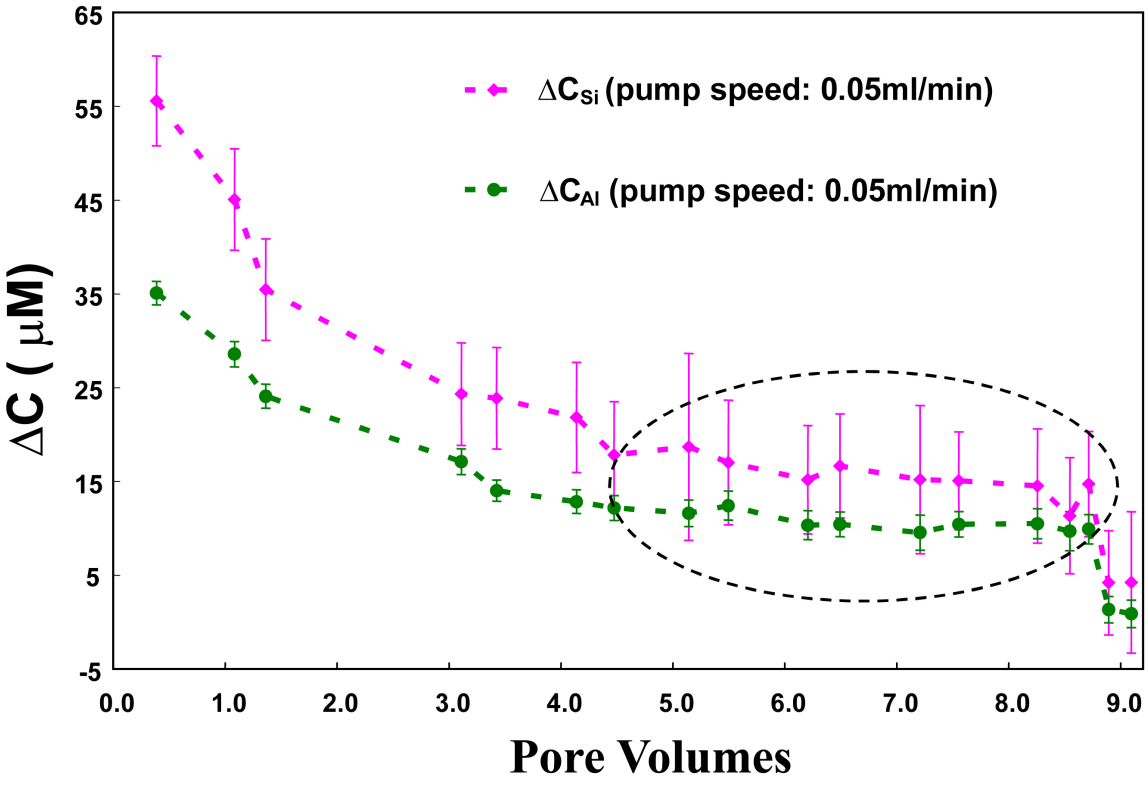
65
55
45
35
25
15
5
-5
ΔC (μM)
0.0
1.0
2.0
3.0
4.0
5.0
6.0
7.0
8.0
9.0
Pore Volumes
ΔCSi (pump speed: 0.05ml/min)
ΔCAl (pump speed: 0.05ml/min)

Figure 6A

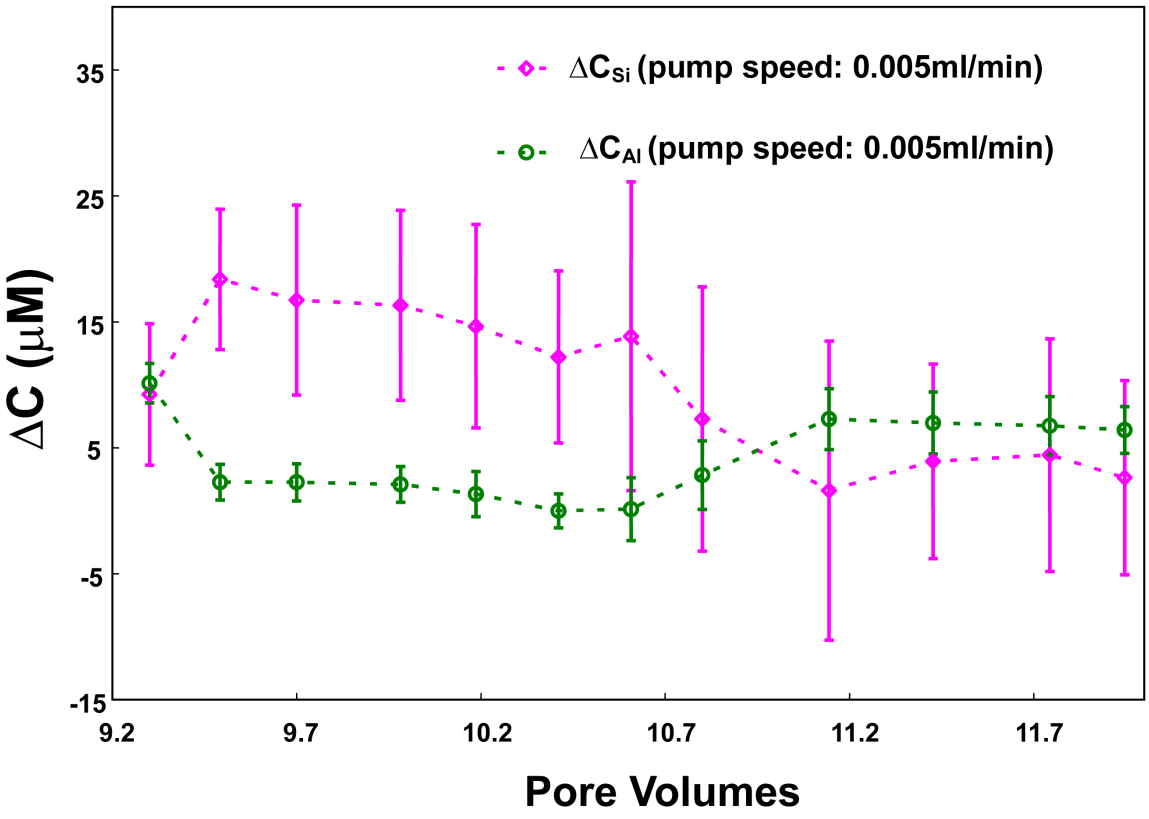
ΔCSi (pump speed: 0.005ml/min)
ΔCAl (pump speed: 0.005ml/min)
ΔC (μM)
35
25
15
5
-5
-15
9.2
9.7
10.2
10.7
11.2
11.7
Pore Volumes

Figure 6B

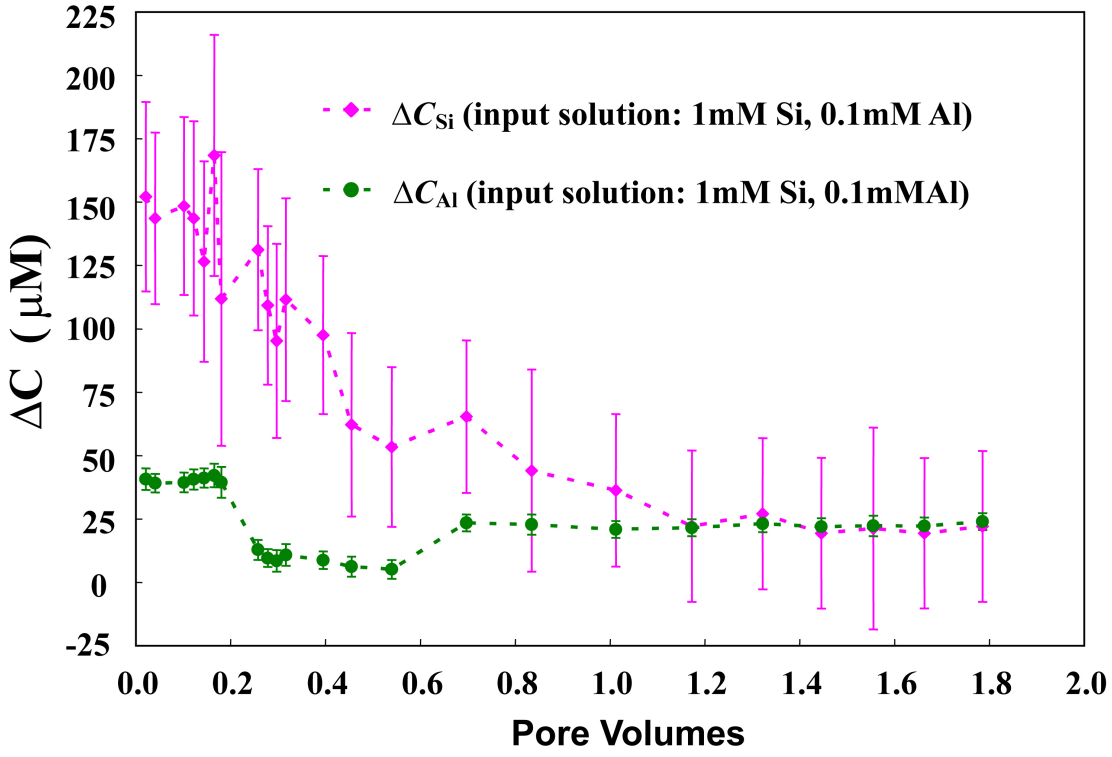
225
200
175
150
125
100
75
50
25
0
-25
ΔC (μM)
0.0
0.2
0.4
0.6
0.8
1.0
1.2
1.4
1.6
1.8
2.0
Pore Volumes
ΔCSi (input solution: 1mM Si, 0.1mM Al)
ΔCAl (input solution: 1mM Si, 0.1mMAl)

Figure 7

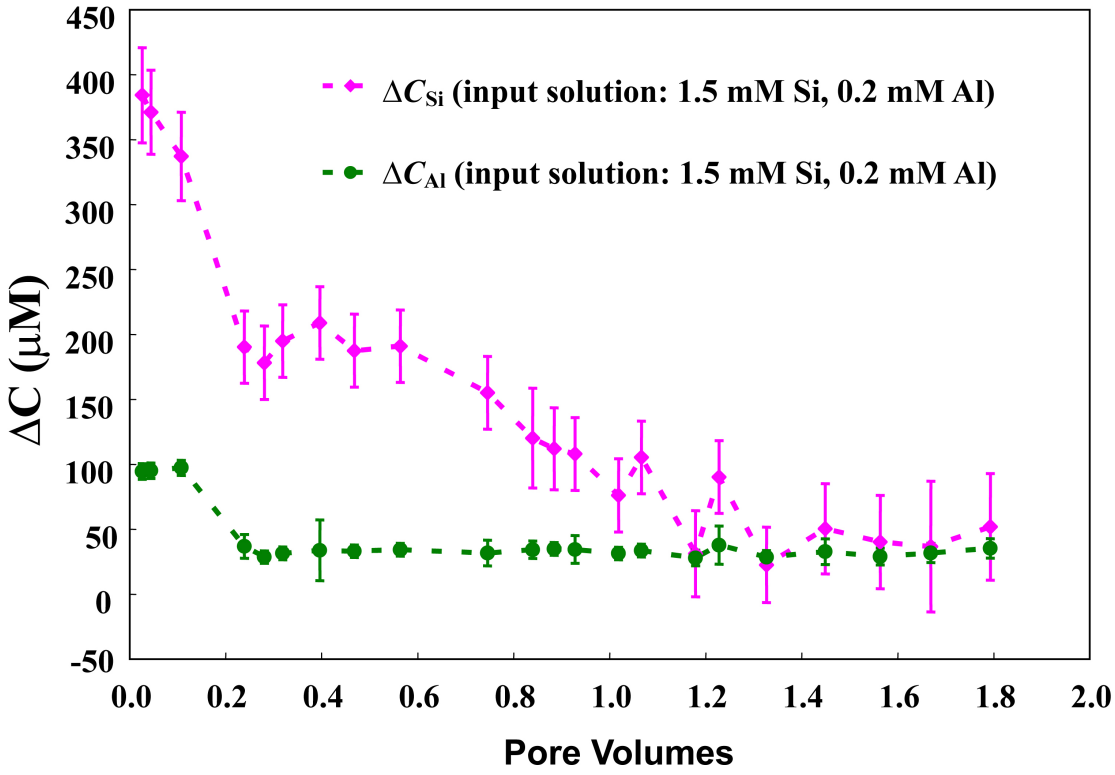
450
400
350
300
250
200
150
100
50
0
-50
ΔC (μM)
0.0
0.2
0.4
0.6
0.8
1.0
1.2
1.4
1.6
1.8
2.0
Pore Volumes
ΔCSi (input solution: 1.5 mM Si, 0.2 mM Al)
ΔCAl (input solution: 1.5 mM Si, 0.2 mM Al)

Figure 8

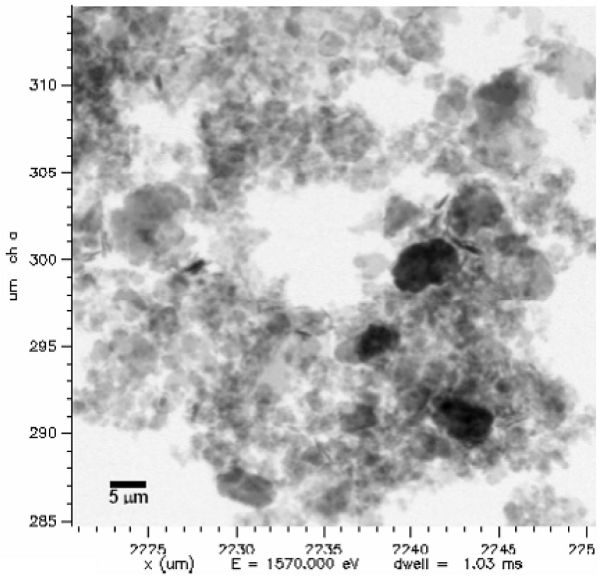

Figure 9A

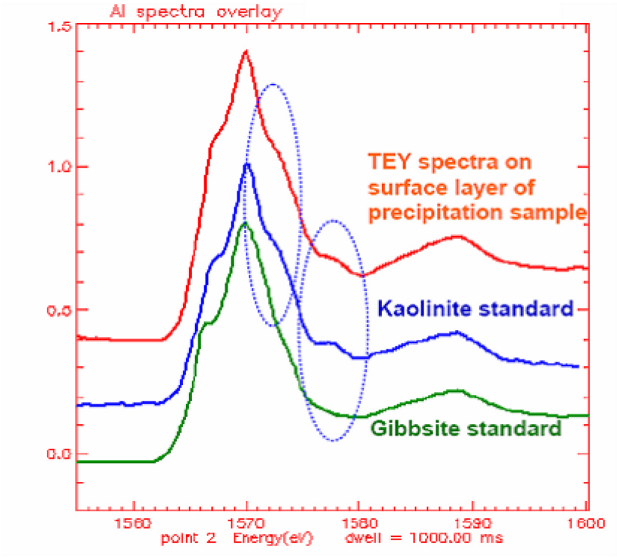

Figure 9B

Figure 9

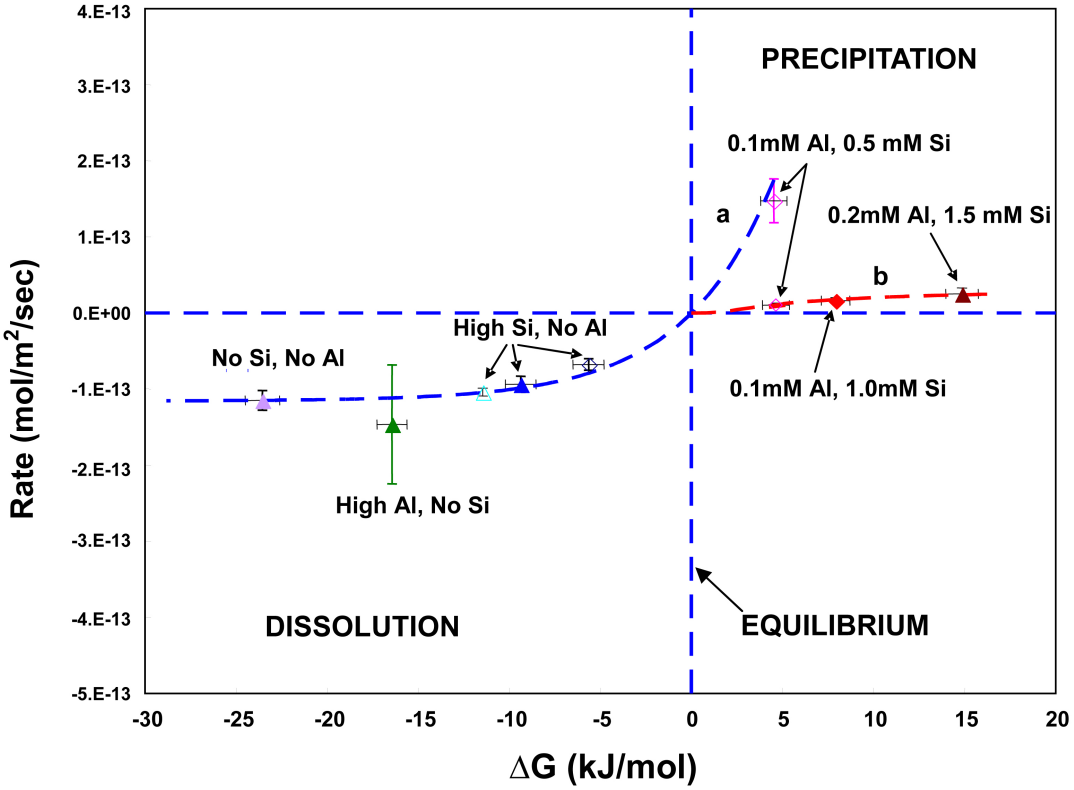
PRECIPITATION
DISSOLUTION
EQUILIBRIUM
0.1mM Al, 0.5 mM Si
0.2mM Al, 1.5 mM Si
0.1mM Al, 1.0mM Si
a
b
No Si, No Al
High Si, No Al
High Al, No Si
Rate (mol/m2/sec)
ΔG (kJ/mol)
4.E-13
3.E-13
2.E-13
1.E-13
0.E+00
-1.E-13
-2.E-13
-3.E-13
-4.E-13
-5.E-13
-30
-25
-20
-15
-10
-5
0
5
10
15
20

Figure 10

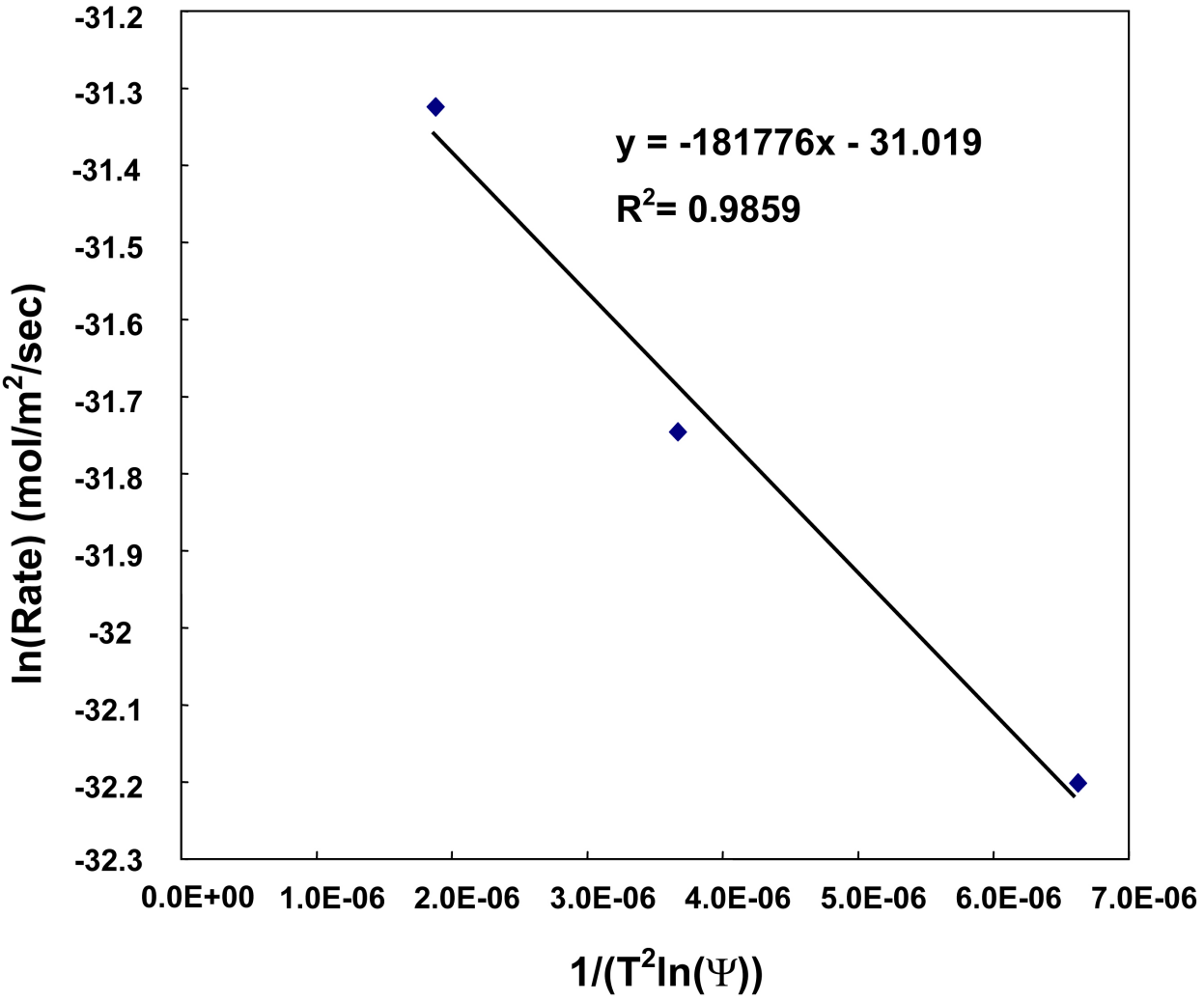
-31.2
-31.3
-31.4
-31.5
-31.6
-31.7
-31.8
-31.9
-32
-32.1
-32.2
-32.3
ln(Rate) (mol/m2/sec)
y = -181776x - 31.019
R2= 0.9859
0.0E+00
1.0E-06
2.0E-06
3.0E-06
4.0E-06
5.0E-06
6.0E-06
7.0E-06
1/(T2ln(Ψ))

Figure 11

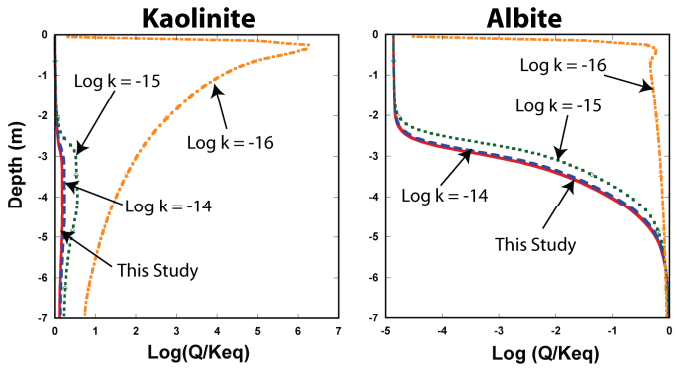
Kaolinite
Albite
Depth (m)
Log k = -15
Log k = -16
Log k = -14
This Study
Log(Q/Keq)
Log (Q/Keq)

Figure 12